Geochemistry, Geophysics, Geosystems

RESEARCH ARTICLE
10.1029/2018GC008161

Explosive Eruptions With Little Warning: Experimental Petrology and Volcano Monitoring Observations From the 2014 Eruption of Kelud, Indonesia

M. Cassidy[1], S. K. Ebmeier[2], C. Helo[3], S. F. L. Watt[4], C. Caudron[5], A. Odell[2], K. Spaans[2], P. Kristianto[6], H. Triastuty[6], H. Gunawan[6], and J. M. Castro[3]

[1]Department of Earth Sciences, University of Oxford, Oxford, UK, [2]School of Environment, University of Leeds, Leeds, UK, [3]Insitute of Geosciences, Johannes Gutenberg University of Mainz, Mainz, Germany, [4]School of Geography, Earth and Environmental Sciences, University of Birmingham, Birmingham, UK, [5]Université Grenoble Alpes, Université Savoie Mont Blanc, CNRS, IRD, IFSTTAR, ISTerre, Grenoble, France, [6]Centre for Volcanic and Geological Hazards Mitigation, Bandung, Indonesia

Key Points:
- Experimental petrology and InSAR data are combined for the first time showing a top-down progression of the Kelud 2014 eruption
- Kelud magmas are stored at shallow depths (2-4 km), mixed volatile conditions precede effusive eruptions, but explosive eruptions are water saturated
- A global monitoring data set demonstrates that explosive eruptions with little warning are common; duration of precursory signals may relate to eruption triggering mechanisms

Supporting Information:
- Supporting Information S1
- Figure S1
- Figure S2
- Data Set S1
- Data Set S2
- Table S1
- Table S2
- Table S3

Correspondence to:
M. Cassidy,
michael.cassidy@earth.ox.ac.uk

Citation:
Cassidy, M., Ebmeier, S. K., Helo, C., Watt, S. F. L., Caudron, C., Odell, A., et al (2019). Explosive eruptions with little warning: Experimental petrology and volcano monitoring observations from the 2014 eruption of Kelud, Indonesia. *Geochemistry, Geophysics, Geosystems*, *20*, 4218–4247. https://doi.org/10.1029/2018GC008161

Received 20 DEC 2018
Accepted 17 JUL 2019
Accepted article online 30 JUL 2019
Published online 29 AUG 2019

©2019. The Authors.
This is an open access article under the terms of the Creative Commons Attribution License, which permits use, distribution and reproduction in any medium, provided the original work is properly cited.

Abstract Explosive eruptions that occur with little or no precursory unrest (less than a month) pose the greatest hazards from volcanoes to nearby populations. Here we focus on the preeruptive conditions for these explosive events, their triggers and how these eruptions evolve. We concentrate on Kelud volcano, where we have conducted a set of petrological experiments to understand preeruptive storage conditions for several recent eruptions. For the 2014 explosive eruption, we combine this with an analysis of interferometric synthetic aperture radar measured deformation. Our data suggest that both explosive and effusive eruptions at Kelud are sourced from a magma storage system at 2–4 km. However, explosive eruptions are fed by magma stored under relatively cool (~1000 °C) and water-saturated conditions, whereas effusive eruptions are fed by slightly hotter (~1050 °C), water-undersaturated magmas. We propose that the initial phase of the 2014 eruption was triggered by volatile overpressure, which then fostered top-down decompression tapping discrete magma bodies. By compiling a global data set of monitoring signatures of explosive eruptions, we show that the onset of unrest rarely points to the shallow ascent of magma to the surface, as ascent mostly occurs in a matter of hours or minutes. We relate the timescale of preeruptive unrest to eruption triggering mechanisms, with yearly/decadal periods of unrest relating to magma injection events (which may or may not precede a magmatic eruption), whereas internal triggering (e.g., second boiling) of an already present, cooling magma body can lead to explosive eruptions with little warning.

1. Introduction

Recent studies suggest that arc magmas can remain in the upper crust for decades to millennia (Rubin et al., 2017), in a mostly crystalline/mushy state (Cooper & Kent, 2014) or even stored as multiple melt-rich lenses from the middle to shallow crust (Edmonds et al., 2016) and that eruption can be triggered rapidly (e.g., Martin et al., 2008). In the most general terms, arc magmas stall in the crust at a point when their density is the same as the surrounding crust (neutral buoyancy). In this model, denser mafic melts normally reside deeper in the crust (Bachmann & Bergantz, 2008), in comparison to felsic melts, which are generally stored at shallower depths within the crust, but may also stall due to their higher viscosities (Annen et al., 2006). In the absence of eruptive records, or for volcanoes that change their eruptive compositions, the depth of inferred magmatic storage alone (from petrological constraints) may provide a first order estimate of eruptive compositions and rheologies, critical for forecasting eruptive behavior (e.g., Muir et al., 2014).

Often eruptions are preceded by long periods (months to years) of preeruptive unrest, but it is still very difficult to forecast the style of an impending eruption. Some suggest that explosive eruptions are usually preceded by short (less than a month) but intense periods of seismicity and/or deformation, which increase in magnitude and rate (e.g., Pallister & McNutt, 2015; White & McCausland, 2016); however, this is not always the case (e.g., Pinatubo 1991, Mt. St. Helens, 1980; Scandone et al., 2007). Linking volcano monitoring data to the processes that cause unrest via retrospective petrological studies can provide further insights into eruptive style controls. Petrological studies note that the conditions at which magmas are stored prior to

eruptions, such as pressure, temperature and volatile content, may also control their explosivity (Joan Andújar & Scaillet, 2012; Cassidy et al., 2016; Koleszar et al., 2012; Owen et al., 2013; Ruprecht & Bachmann, 2010). Generally, whether a volcano erupts effusively or explosively is thought to be a product of how efficiently the magma can outgas, which is related to its viscosity and the rate at which it decompresses and ascends (Cassidy et al., 2018; Eichelberger et al., 1986; Gonnermann & Manga, 2007; Jaupart & Allègre, 1991). These parameters all differ depending on the conditions and processes that occur while in storage. Fast ascent will limit outgassing (known as closed-system degassing) thus increasing explosive potential, and this could be controlled by the conditions magmas endure while in storage, how the eruptions are triggered or how they evolve (i.e., changes in overpressure, degree of outgassing and storage conditions). As an eruption progresses these parameters will change and may lead to transitions in eruptive style (Eichelberger et al., 1986; Jaupart & Allègre, 1991). Monitoring how the magmatic properties evolve throughout an eruption has the potential to help us forecast eruptive style transitions and when the eruption will end.

Forecasting explosive eruptions is one of the key aims of volcanology, due to their potential for large losses of life. Monitoring geophysical and geochemical signals is the basis for short to medium term forecasting and for detecting changes during an ongoing eruption (Tilling, 2008). The duration and character of preeruptive unrest therefore largely determines our ability to make forecasts. At some volcanoes, unrest in the form of elevated seismicity, deformation, gas, and heat flux, can last for months to years (e.g., Soufriere Hills; Druitt et al., 2004), while at others the transition from quiescence to eruption is rapid, lasting only days to hours, leaving the nearby populations with little time to prepare (e.g., Calbuco; Castruccio et al., 2016). Passarelli and Brodsky (2012) show that higher silica eruptions have generally longer run-up times; longer repose periods and erupt larger volumes of material, which they attribute to higher magma viscosities. Phillipson et al. (2013) analyze monitoring records from the Smithsonian Institution Global Volcanism Program between 2000 and 2011 and suggest a relationship between unrest periods and volcano type, with calderas and shield volcanoes having on average longer periods of unrest than stratovolcanoes.

The duration of preeruptive unrest may also be linked to magma storage conditions (such as temperature, pressure, crystal, and volatile contents), fast ascent rates, and their triggering mechanisms. For instance, a magma recharge eruption trigger may be associated with months of seismicity during magmatic ascent (e.g., Pinatubo, Pallister et al., 1992), uplift of the Earth's surface caused by elastic deformation (e.g., Lu & Dzurisin, 2014), and elevated gas fluxes or ratios derived from recharging magmas (e.g., Merapi, Surono et al., 2012). In contrast, eruptions that are triggered "internally" by volatile overpressure (Blake, 1984), magma buoyancy (Caricchi et al., 2014), late stage volatile saturation (Stock et al., 2016), and decompression (or top-down triggering, e.g., Alidibirov & Dingwell, 1996; Tarasewicz et al., 2012) and the onset of degassing (Girona et al., 2016) may not be associated with long periods of magma movement that cause measurable geophysical signals (Petrelli et al., 2018). Retrospectively classifying rapid-onset eruptions is challenging, as it requires geophysical or geochemical gas measurements with sufficient temporal resolution to have captured any preeruptive signals. Expansion and densification of ground-based instrumentation and the tasking of particular satellite instruments often occurs after the onset of eruptions, so that historical monitoring records tend to be biased in coverage of coeruptive and posteruptive periods (e.g., Figure 4 in Biggs et al., 2014). However, the increase in the number of volcanoes being continuously or regularly monitored, together with developments in remote sensing (e.g., background satellite missions, continuously recording infrasound), means that very brief periods of preeruptive unrest can be identified for several eruptions over the past decade (e.g., Chaiten, 2008; Colima, 2015; Rabaul, 1995; Redoubt, 1989; Reventador, 1999; Ruapehu, 1996, and eruptions from Hekla, Kilauea, Piton de la Fournaise, Usu. Pavlof, and Calbuco; Lesage et al., 2018; Matoza et al., 2018; Passarelli & Brodsky, 2012).

Here we use experimental petrology to reconstruct the preeruptive storage conditions prior to several explosive and effusive eruptions at Kelud volcano, Indonesia, a basaltic-andesitic arc stratovolcano that has erupted several times over the past century, with styles ranging from intense Plinian explosive eruptions to lava dome extrusion (Triastuty et al., 2014). For the 2014 explosive eruption our petrological analysis is supplemented by satellite radar and seismoacoustic measurements to investigate evidence for magma movement during the buildup and progression of the eruption. Our data show that magma can reside almost undetected in a shallow magma reservoir in the immediately preeruptive period (cf. Krafla; Elders et al., 2011) and that explosive eruptions can be triggered internally, without need for a magmatic injection trigger.

1.1. Geological Background

Kelud (often referred to as Kelut) sits on top of a subduction system, which stretches from northwest Sumatra to Java and through to Flores in the east. Volcanism in Java is formed from the subduction of the Indo-Australian plate beneath the Eurasian plate at a rate of 6–7 cm/year (DeMets et al., 1990; Tregoning et al., 1994). Kelud is situated in central-east Java, near the locus of subduction of the Roo Rise submarine topographic ridge (Kopp et al., 2006), leading to subduction erosion and consequently lower subducted sediment signatures compared to the west (Plank & Langmuir, 1998).

Kelud's summit elevation is 1,731 m above sea level, and its irregular stratocone structure includes remnants of lava domes, craters, and two avalanche calderas, one open to the south and the other to the west, within which is the active crater (Bourdier et al., 1997). The western half of the volcano comprises debris avalanche deposits several hundreds of meters thick from slope failure of the western flank (Bourdier et al., 1997; Thouret et al., 1998).

Kelud is one of the most dangerous volcanoes in Indonesia, located in populous Java where over 2 million people live within 30 km and over 50,000 within 10 km of the volcano (Global Volcanism Program, Smithsonian Institution (2013); Loughlin et al., 2015). There have been eight eruptions over the last 100 years (1919, 1920, 1951, 1966, 1967, 1990, 2007–2008, and 2014) killing over 6,000 people, and more than 30 eruptions during the past six centuries that have claimed the lives of 15,000 victims from lahars, pyroclastic density currents, and ash fall (Kusumadinata, 1979). Since 1901, an eruption has occurred every 13 years on average (Nakamichi et al., 2017). Eruptive durations have normally been short (a few hours) and eruptions have been moderate in magnitude: VEI 4 (Volcanic Explosivity Index) for the explosive eruptions, with ~0.1–0.3 km^3 of tephra per eruption (Bourdier et al., 1997; Goode et al., 2018; Nakamichi et al., 2017). The average rate of extrusion of magma at Kelud during the twentieth century estimated from cumulative volumes of mapped deposits is 2×10^6 m^3/Y (Dense Rock Equivalent (DRE); Ishihara et al., 2011). Kelud regularly changes its style of eruptions with some exhibiting fully effusive behavior (1376, 1920, 1967, and 2007), and others solely explosive (e.g., 1586, 1901, 1919, 1951, 1966, 1990, and 2014; Goode et al., 2018).

As a product of the frequent and dynamic eruptions, the morphology of the crater area of Kelud changes significantly. During periods of quiescence a crater lake develops, fed by the underlying hydrothermal system (Bernard & Mazot, 2004), which is generally then expelled during eruptions (e.g., 1990). Large numbers of deaths in the eruptions can be attributed to water displaced from the crater lake producing primary lahars (Thouret et al., 1998). Therefore, since the 1919 eruption, the lake volume has been partially drained to reduce this risk (Badrudin, 1994). Due to this lake drainage, no primary lahars were produced in the 1951 and 1990 eruptions and the casualties were consequently lower. During the 2007–2008 eruption a dome filled the crater displacing some of the lake, and both the dome and the lake were evacuated during the 2014 explosive eruption. Since the 2014 eruption, the crater is again being filled in by a lake, which, as discussed below, can be useful to detect signals of increasing magmatic activity via hydroacoustic noise and changing lake chemistry and temperature (Lesage & Surono, 1995; Vandemeulebrouck et al., 2000).

1.2. Eruptions and Unrest Since 1990

Kelud's most recent eruptions (1990, 2007–2008, and 2014) were monitored and successfully forecasted by the Center for Volcanology and Geological Hazard Mitigation (CVGHM) in Indonesia. The 1990 eruption was preceded by 4 months of unrest, comprising seismic activity, increase of lake temperature, decrease in pH, and changing lake chemistry, along with acoustic noise in the crater and lake, attributed to the influx of volcanic gases and increased pressure and temperature within the underlying hydrothermal system (Badrudin, 1994; Lesage & Surono, 1995; Vandemeulebrouck et al., 2000). The seismicity consisted of an average of eight events per day of mostly shallow volcano tectonic (VT, most likely <1 km directly below the crater) earthquakes producing low cumulative seismic energy (5.6×10^8 J) in the lead up to the eruption. Seismicity returned to a very low level in the 3 weeks prior to the eruption, followed by a 24-hr period before the eruption when the seismicity increased rapidly, and tremor began (Lesage & Surono, 1995). The seismicity is thought to be linked to the gradual fracturing of a solid body (thought to be cooled residual magma from the 1966 eruption) within the eruptive conduit, the low seismic energy showing that the plug did not offer strong mechanical resistance (Lesage & Surono, 1995). In addition to seismicity, changes in the

crater lake were recorded 4 months prior to the eruption including, decreased pH, increased temperature, and concentrations of sulfate, boron, magnesium, chloride and Mg/Cl ratio, these changes were attributed to influx of magmatic-derived fluids into the lake (Badrudin, 1994). The eruption started on 10 February 1990 at 11:41 (local time) with a series of phreatic eruptions, followed an hour later by Plinian/sub-Plinian column, which was sustained for several hours and rose to 10 km (Lesage & Surono, 1995). The eruption lasted 4 hr in total and produced 0.12 km^3 of tephra with an eruptive rate of 7.5×10^6 kg/s (Bourdier et al., 1997).

The effusive dome-forming eruption of 4 November 2007 was preceded by several months of unrest. In August of that year, an echo-sounding survey together with floating accumulation chamber measurements detected abnormally high carbon dioxide emissions (Caudron et al., 2012). Soon after these measurements, the lake temperature and conductivity started to increase. Seismicity rose in September and changes in lake color and chemistry prompted the CVGHM to create a 5-km evacuation zone. A regional L-band interferometric synthetic aperture radar (InSAR) survey did not detect deformation prior to the eruption (Philibosian & Simons, 2011). However, tiltmeter data from the crater rim showed continuous uplift from July to the beginning of September and the depths of VT earthquakes ranged from 5 km to just beneath the crater during this period (Hidayati et al., 2011, 2018). The VT earthquakes stopped several days before the eruption and were replaced by low magnitude 'drumbeat' like seismicity (Nakamichi et al., 2017). Following this was an 8-hr period of quiescence and then continuous tremor until a phreatic eruption. The authorities were expecting an explosive eruption; however, between November 2007 and May 2008 a 3.5×10^7 m^3 lava dome grew in the crater. Following the eruption in late 2008, there was a possible maximum 15 cm line-of-sight displacement detected in InSAR data, although this is based on only two radar acquisitions, so doubts exist about whether this was permanent, real deformation (inflation) rather than a short term atmospheric effect (Philibosian & Simons, 2011).

Before the explosive eruption on 13 February 2014, the seismicity, dominantly comprising distal VTs, was at a low level throughout January, gradually increasing until a peak on 2 February, reaching 117 events/day (Global Volcanism Program, Smithsonian Institution (2013); Nakamichi et al., 2017). The seismicity then decreased for the following 4 days before dramatically increasing from 7 February until the eruption on 13 February. The hypocenters of the seismicity were located centrally, 1–2 km below the bottom of the crater (Triastuty et al., 2014). One tiltmeter showed gradual uplift of the crater area from December 2013 until 2 hr before the eruption, and the small crater lake showed an increase in temperature of 4 °C from January 2014; however, it is noted that single stations may record spurious signals (Nakamichi et al., 2017; Sri Hidayati et al., 2018; Triastuty et al., 2014). On 2 February, alert levels were changed from level 1 (normal) to level 2 (advisory), changing to level 3 (watch) on 10 February, and such was the fast ramp up of seismic activity in the last days, it was changed to level 4 (warning) only 90 min before the eruption. This contrasted with the activity of 2007 where levels 3 and 4 were raised 5 and 3 weeks prior to the eruption, respectively (Nakamichi et al., 2017). The total seismic energy preceding the 2014 eruption was an order of magnitude higher (2.2×10^9 J) than the seismicity build up in 2007 (3×10^8 J), which also reflects the relative difference in their erupted volume (Nakamichi et al., 2017).

The eruption started at 22:45 local time (15:45 UTC) with the destruction of the 2007–2008 dome, generating high-energy pyroclastic density currents (PDCs) toward the NE to a distance of ~7 km. The ballistic ejecta and PDCs destroyed all the local monitoring instruments (Goode et al., 2018; Maeno et al., 2016). This stage was associated with a brief infrasound signal followed by a weak seismic event indicating a small-scale eruption (Caudron et al., 2015). The second stage of the eruption occurred ~15 min later with the production of a sustained Plinian column reaching an altitude of 26 km, with most of the ash injected 16–17 km into the atmosphere (Kristiansen et al., 2015). This umbrella cloud spread over a large region, with the diameter spreading to 200 km in less than 2 hr (Maeno et al., 2016). Seismicity suggests that this Plinian stage lasted ~2 hr before the eruption column became unstable and later collapsed (Caudron et al., 2015). The last stage of the eruption marked the end of the main Plinian phase, producing pumice-rich PDCs as the Plinian column collapsed (Maeno et al., 2016). The eruption waned in energy producing a low-altitude plume affected by lower level SW winds, distributing fine ash across the villages northeast of the volcano. This led to multiple roof collapses in Malang district, as observed in photos and reports. The mass eruption rate was between 3×10^7 and 1×10^8 kg/s (Maeno et al., 2016; Suzuki & Iguchi, 2017). Seismic and infrasound

data suggest the eruption had an estimated intensity between that of Mount St. Helens (1980, Washington State, United States) and Pinatubo (1991, Philippines; Caudron et al., 2015), despite a total volume (0.14–0.28 km^3 in dense rock equivalent) that was an order of magnitude smaller than these events.

2. Materials and Methods

In this section we describe the collection of samples, our experimental and analytical setup, how our monitoring data, for example, satellite data, seismic, and infrasound data was acquired. This multiparameter data set aims to help constrain the storage conditions of Kelud magmas, and the monitoring data will help to piece together the presence of prior unrest and the progression of the 2014 eruption.

2.1. Field Samples

The study uses samples from five different locations for the following eruptions; 2014 main and late phase (low altitude plume phase), 2007, 1990, and an older explosive eruption (undated). These eruptive products were sampled around Kelud during an expedition in 2015 with the assistance of the Kelud volcano observatory in Margomulyo (Figure 1). The 2014 main-phase pumices and 2007 dome rocks were sampled near the crater rim and the 2014 late-phase ash NE of Kelud from a 10- to 11-cm-thick dark ash deposit with fine pumice lapilli. The 1990 eruptive products were sampled by digging a hole in a highly vegetated area SW of the volcano. This ~28-cm thick deposit was 11 cm below the surface, underlying a thin pumice fall deposit of 2014 and a 7 cm soil horizon. The deposit comprised a fine, phreatomagmatic ash at the bottom (~5 cm), and above this a normally graded 15-cm thick coarse pumice lapilli unit, followed by an 8-cm thick deposit of finer pumiceous material. This deposit comprised both light and dark ("scoria") pumice clasts as observed by Bourdier et al. (1997). An older explosive eruption was sampled 0.5 m from the top of a small escarpment 9 km west of Kelud and comprised a 37-cm thick deposit of well sorted, angular pumice fall. Its stratigraphic position and lithofacies differed from the 1990 eruption (no scoria), but it may be associated with a more voluminous historical explosive eruption (e.g., 1901, 1826, and 1586; Goode et al., 2018).

2.2. Experimental Setup

Experiments were undertaken to constrain the magma storage conditions prior to different eruptions at Kelud. A gas-pressurized TZM (Tungsten Zirconium Molybdenum) cold-seal pressure vessel was used, with Argon as the pressurizing medium. Due to the crystal-rich nature of the basaltic andesite, coarsely crushed aliquots of the 2014 Kelud pumice was used as starting material, to achieve partial equilibrium as in Pichavant et al. (2007). This approach of "partial equilibrium" retains the antecrystic cores (<10% in the case of Kelud; Cassidy et al., 2016), so that only the glass and the crystal rims reacted in the experiments, in order to achieve equilibrium with glass and mineral rims, with the crystal cores acting also as nucleation sites. Two "reverse" or "crystallization" experiments were conducted, where we heated the starting material above liquidus, thus mixing all crystal cores with the magma, and then returned it to a cooler equilibrium temperature. When comparing these with our standard experiments conducted at the same conditions, we were not able to replicate the same matrix glass and mineral data (supporting information), reinforcing our approach not to crush our crystal cores with the reactive magma. Approximately 0.1 g of sample was inserted into a $AgPd_{30}$ capsule, together with distilled water using a micro syringe, enough to saturate the magma in H_2O at the pressure and temperature of the experiments. For mixed volatile experiments $AgCO_3$ powder was added in specific molar proportions along with water, to generate water fractions ($XH_2O = H_2O/(H_2O + CO_2)$) in the fluid phase from 0.55 to 0.75. To buffer the fO_2 conditions to NNO, CH_4 was added as a pressurizing gas (0.4-MPa partial pressure) and a double-capsule technique was employed (Shea & Hammer, 2013), whereby Nickel powder was added to a platinum foil capsule and left open to buffer the magma. Ni powder (grey) oxidizes to green during oxidation to NiO; therefore, the capsules were checked at the end of the experiment to ensure that both green and grey powder were still present. The sample was welded on both ends using an acetylene and oxygen flame, with the capsule in contact with water to limit capsule heating. The capsule was weighed again, to ensure no volatiles were lost during the welding process. The $AgPd_{30}$ capsules were inserted into the sample holder attached to a magnet, which was inserted into a TZM autoclave, achieved by raising the external magnet up into the hottest part of the autoclave. A K-type thermocouple was inserted into a small hole in the end of the autoclave close to the capsule position to check for temperature offset between the furnace's internal thermocouple and autoclave. The samples were held at P and T commensurate with upper crustal conditions (e.g., 950–1100 °C; 25–200 MPa; Figure 2 and

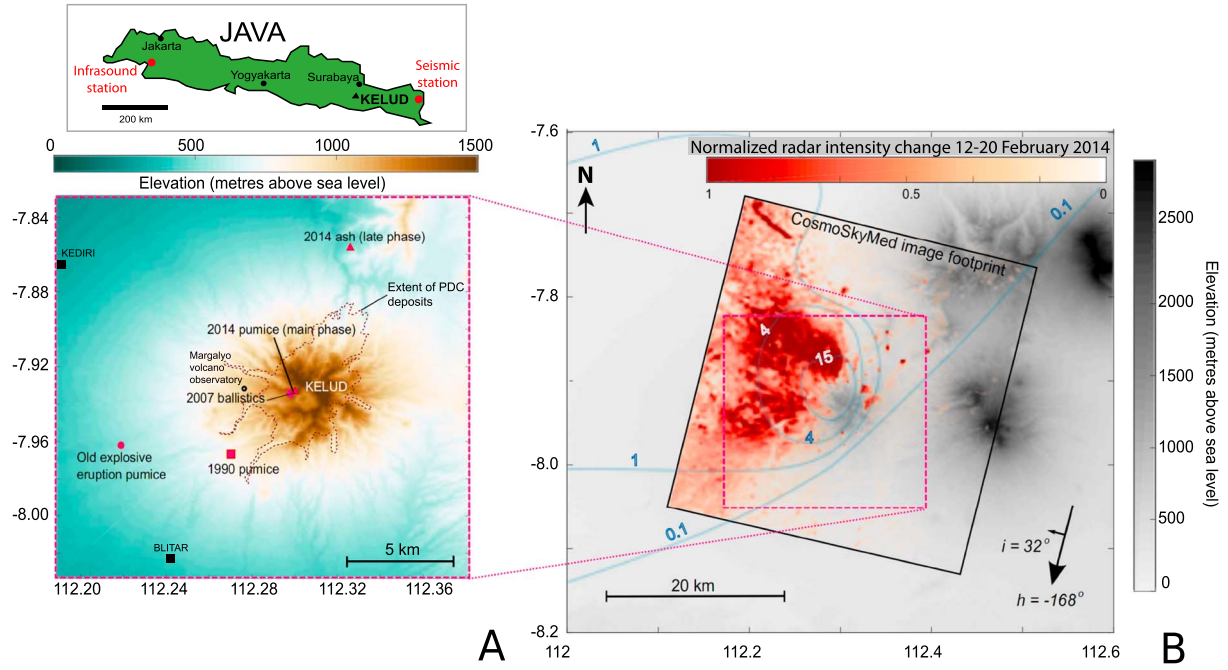

Figure 1. (a) Topographic map of Kelud volcano with sampling sites indicated. (b) The footprint of the descending CosmoSkyMed images used in our analysis (heading = −168°, incidence angle = 32°) shown with scaled synthetic aperture radar intensity difference between 12 and 20 February 2014 ($\sigma_{before} - \sigma_{after}$). Higher values (reds and oranges) therefore indicate a decrease in intensity, which we attribute to ashfall. Blue contours are traced from Maeno et al. (2016) and represent isopachs of ash fall thickness (in cm) derived from field measurements.

supporting information Table S1) for 1 to 3 days to equilibrate (Table S1) and then rapidly quenched by lowering the external magnet so that the sample was drop quenched as it entered a water-cooled coupling system to prevent further crystallization. Both H_2O-saturated and mixed H_2O-CO_2 conditions were explored in this study (Figure 2 and Table S1).

2.3. Analytical Methods

Aliquots of the natural samples were crushed and milled for X-ray fluorescence analysis. Major elements were analyzed on glass beads prepared by fusion of a mixture of 0.5-g subsamples and lithium tetraborate in a ratio of 1:10. Minor elements were made into pellets using a press. Analyses were undertaken using a Philips MagiXPRO spectrometer with a rhenium X-ray tube at the Johannes Gutenberg University, Mainz, Germany. Error and external accuracy (relative standard error) was <2% for all elements.

The samples were also made into polished thin sections and resin mounts, and then carbon coated for use in a Zeiss DSM 942 scanning electron microscope (SEM) and electron microprobe analysis (EMPA) on a JEOL superprobe at the Johannes Gutenberg University, Mainz. All quantitative EMPA analyses used an accelerating voltage of 15 kV. For plagioclase and pyroxene analyses a spot size of 4 μm and a 100 nA beam current was used. Rims of crystals were analyzed, where we can discern a difference rim growth from Back scatter electron (BSE) images (e.g., supporting information Figure S2). For glasses, a 10-μm defocused spot was used with a beam current of 10 nA, with counting times of 50–200 s per analysis. During glass measurements, Na peaks were counted first to avoid significant migration during the run. In the 2007 eruptive products, most melt inclusions were crystallized or considerably affected by post entrapment crystallization, so to generate a more representative preeruptive composition (prior to microlite crystallization), 50-μm spots of were used over areas of groundmass mixed glass and microlites, the average and standard deviation was calculated from 23 data points. As the groundmass was dominated by plagioclase crystals, the matrix effects will be limited, due to similar values for fluorescence, absorption, and atomic number between plagioclase and glass. A Phi-rho-Z correction for atomic number, absorption, and fluorescence was automatically applied to all analyses, and the calibration was performed using a range of natural and synthetic standards. One sigma standard deviations were generally less than 2% for most major elements analyzed.

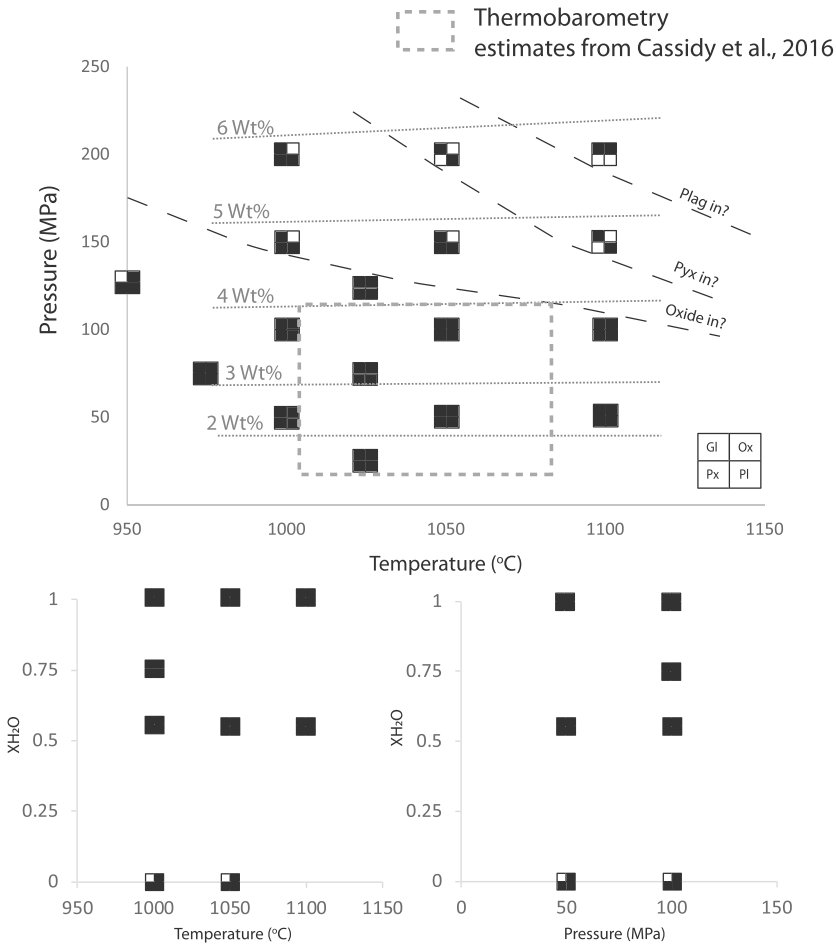

Figure 2. Experimental conditions explored in this study. (a) Water saturated experiments. The white boxes signify absence of a phase, and black box signifies presence. Water content lines are produced uisng the glass chemistry, P and T conditions using the Papale et al. (2006) solubility model. (b and c) Mixed volatile experiments at differing conditions.

To estimate the proportion of different mineral phases present in the natural and experimental products, energy dispersive spectrometer (EDS) mapping was conducted on an Oxford instruments detector on the SEM at the University of Mainz. Al, Ti, and Mg maps were made for plagioclase and glass and Ca and Na maps for pyroxene. At least three maps of 1,024 × 1,024 pixel areas (at 70 frames each) were taken for each sample, using a similar method to Muir et al. (2012). Image J was then used to threshold and calculate the relative proportions of glass, plagioclase, pyroxene and oxides (supporting information Table S1). Backscattered electron images of thin sections at varying magnifications were taken with the SEM to measure bubble number densities via the FOAMS program following the method of Shea et al. (2010).

2.4. Satellite Radar Measurements

InSAR allows the measurement of displacements of the Earth's surface using pairs or sets of time-separated radar images (e.g., Simons & Rosen, 2015). At volcanoes, InSAR has been used to investigate deformation attributed to the movement of magma and magmatic fluids, variations in pressurization of a magmatic or hydrothermal reservoir and the alteration of erupted material (e.g.,Biggs & Pritchard, 2017 ; Ebmeier et al., 2018 ; Pinel et al., 2014). At Kelud, we analyze a set of 30 X-band (wavelength = 0.031 m, pixel size = ~3 m) COSMO-SkyMed images spanning between 2 December 2013 and 19 May 2014.

InSAR measurements of displacement are derived from phase differences between radar images and used to produce maps of displacement ("interferograms"). When either changes in satellite position (characterized by perpendicular baseline) or changes in surface scattering properties are too great, phase becomes

incoherent, and displacements cannot be retrieved. Dense vegetation, and particularly Kelud's steep topography, contributes to low coherence, which prevent measurements on the edifice itself, even in the preeruptive period. The 2014 eruption destroyed the dome from the 2007 event, created a new summit crater, killed the surrounding vegetation, and blew down trees over an area >10 km^2. During the first stage of the eruption, high-energy PDCs disturbed the area surrounding the summit, while pumice-rich PDCs from later in the eruption filled valleys on all sides of the volcano and extend >6 km, beyond the area affected by earlier phases (Maeno et al., 2016; Figure 1). This complete alteration of scattering properties made measurements of coeruptive displacement within ~7–8 km of Kelud's summit impossible. Our deformation observations spanning the eruption are therefore limited to stable scatterers away from the volcanic edifice. We use changes in radar intensity between 12 and 20 February 2014 to illustrate the distribution of ash fall, which in this case caused a decrease in the proportion of microwave radiation reflected back to the satellite and a decrease in intensity (Figure 1b).

We take a persistent scatterer approach (Ferretti et al., 2011; Hooper et al., 2004) to processing, initially based on a set of single master interferograms (master date = 8 February 2018, perpendicular baseline magnitudes from 0.4 m to 1,157 m, mean = 560 ± 340 m). Topographic phase contributions were corrected using the TanDEM-X WorldDEM (12-m spatial resolution, released 2014). Due to the low number of persistent scatterers identified by our initial analysis using StAMPS (Hooper et al., 2004), we then reanalyzed the data using points selected on the basis of ensemble coherence rather than time series methods (RapidSAR, Spaans & Hooper, 2016). RapidSAR identifies groups of pixels that share a similar scattering mechanism ("siblings") and uses the resulting coherence estimate to predict coherent points individually for each interferogram. After coregistration of all the images, a set of interferograms were constructed for each image, greatly increasing the number of points in our analysis.

We constructed a time series of a small-baseline subset of RapidSAR interferograms (Data Set S1) to find the incremental displacements between image acquisition dates (e.g., (Berardino et al., 2002; Schmidt & Bürgmann, 2003). We used a least squares inversion, fitting the minimum constraint to velocity over each time interval, and treat the first date in the time series as a reference time when no deformation was taking place. We solve for a linear ramp in each interferogram, but make no corrections for atmospheric contributions to phase.

2.5. Infrasound and Seismic Data

Due to the lack of available local (<15 km from the volcano) observations, we have to rely on remote seismoacoustic records, which provide a timeline for the eruption. Volcanic eruptions often radiate low-frequency seismoacoustic energy (<1.0 Hz) that can propagate over large distances from a volcanic vent. Several remote geophysical instruments detected the 2014 Kelud eruption permitting to study its chronology and estimate its intensity (Caudron et al., 2015; Nakamichi et al., 2017). Three distinct low-frequency signals were detected by remote seismic stations while acoustic waves were recorded twice by several infrasound arrays of the International Monitoring System network (Caudron et al., 2015) and as total electron content variations by several satellites (Nakashima et al., 2016). Our analyses include the use of the ObsPy software (Krischer et al., 2015).

3. Results

3.1. Natural Eruptive Products

The whole rock data for recent and historic eruptions (1990, 2007, 2014) comprise near identical chemical compositions of basaltic andesite at ~54 to 55 wt% SiO_2, consistent with previous studies (e.g., Jeffery et al., 2013). The phenocryst contents are consistently high at ~50–60% (Cassidy et al., 2016), and matrix glass and melt inclusions are dacitic in composition (Figure 3). Melt inclusions were chosen on their glassy, crystallized, and noncracked characteristics from multiple, nonantecryst (<90 An cores) plagioclase phenocrysts. The plots on figure 3 show overlapping compositions for the natural eruptive products used in this study: 2007, 1990, 2014, and late 2014, and a voluminous undated pumice fallout deposit, hereafter referred to as the older explosive eruption. However, the older explosive eruption comprises ~1 wt% lower concentrations for MgO, CaO, and Al_2O_3. Along with whole rock compositions, also plotted in Figure 3 are matrix glass and melt inclusions compositions for the natural products used in this study. There are

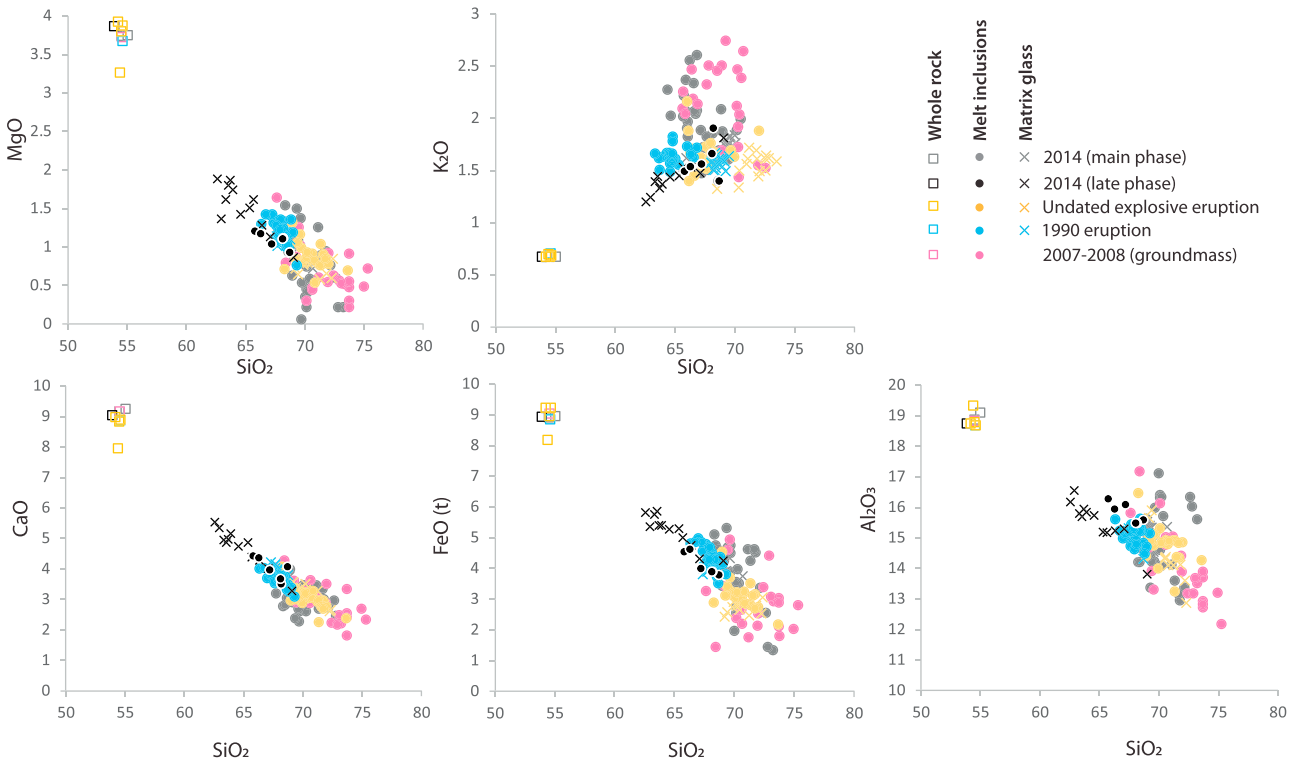

Figure 3. Geochemistry plots of melt inclusions, matrix glass, and whole rock data for recent and older eruptions at Kelud.

broad negative correlations for most oxides versus SiO_2, apart from K_2O, where a weak positive correlation exists. The matrix glass data plot mostly at higher CaO, FeO, Al_2O_3, and MgO contents relative to melt inclusions. The most mafic of these are from the late 2014 eruption, while the most evolved are from the older explosive eruption. The melt inclusion compositions form in closely packed clusters. The averaged EMPA spots of 2007 groundmass are more scattered and extend to the highest SiO_2 contents. There is a variation in melt inclusions compositions between the 2014 main eruption phase and the later erupted products, generally becoming more primitive and less silicic. The matrix glass contents for the main phase of the 2014 eruption overlap in composition with the 2014 melt inclusion compositions (grey symbols in Figure 3); however, there is a deviation in the late 2014 matrix glass and melt inclusion compositions (black symbols), which extend to less evolved compositions.

3.2. Experimental Constraints on Magma Storage Conditions

The consistent whole rock composition of the natural eruptive products (Figure 3) allows us to apply our experimental petrology data constraints to multiple eruptions, with the assumption that the initial source magma compositions were more or less the same. Chemical compositions and phase proportions of experimental glass and minerals are plotted along with the natural eruptive compositions (mostly melt inclusion compositions) for comparison in Figures 4–7. As this was not a typical "phase equilibria" study (instead "partial equilibrium"), the presence or absence of minerals was not a reliable indicator of exact conditions, since some of these phases were present in the starting material. We therefore did not use this approach to attain preeruptive storage constraints, but instead used the chemical compositions of glass and mineral rims of the natural samples to match those in the experimental products (e.g., Erdmann et al., 2016). Nevertheless, we have noted the presence of mineral phases in Figure 2 and Table 1, which provide some coarse constraints regarding the P-T conditions that could not replicate the natural phase assemblage of plagioclase, orthopyroxene, clinopyroxene, magnetite, and glass (supporting information Figure S1). It shows that some of the natural mineral phases were not stable at conditions above 125 MPa, and temperatures below 975 °C, thus providing some initial constraints on P-T conditions of the Kelud products.

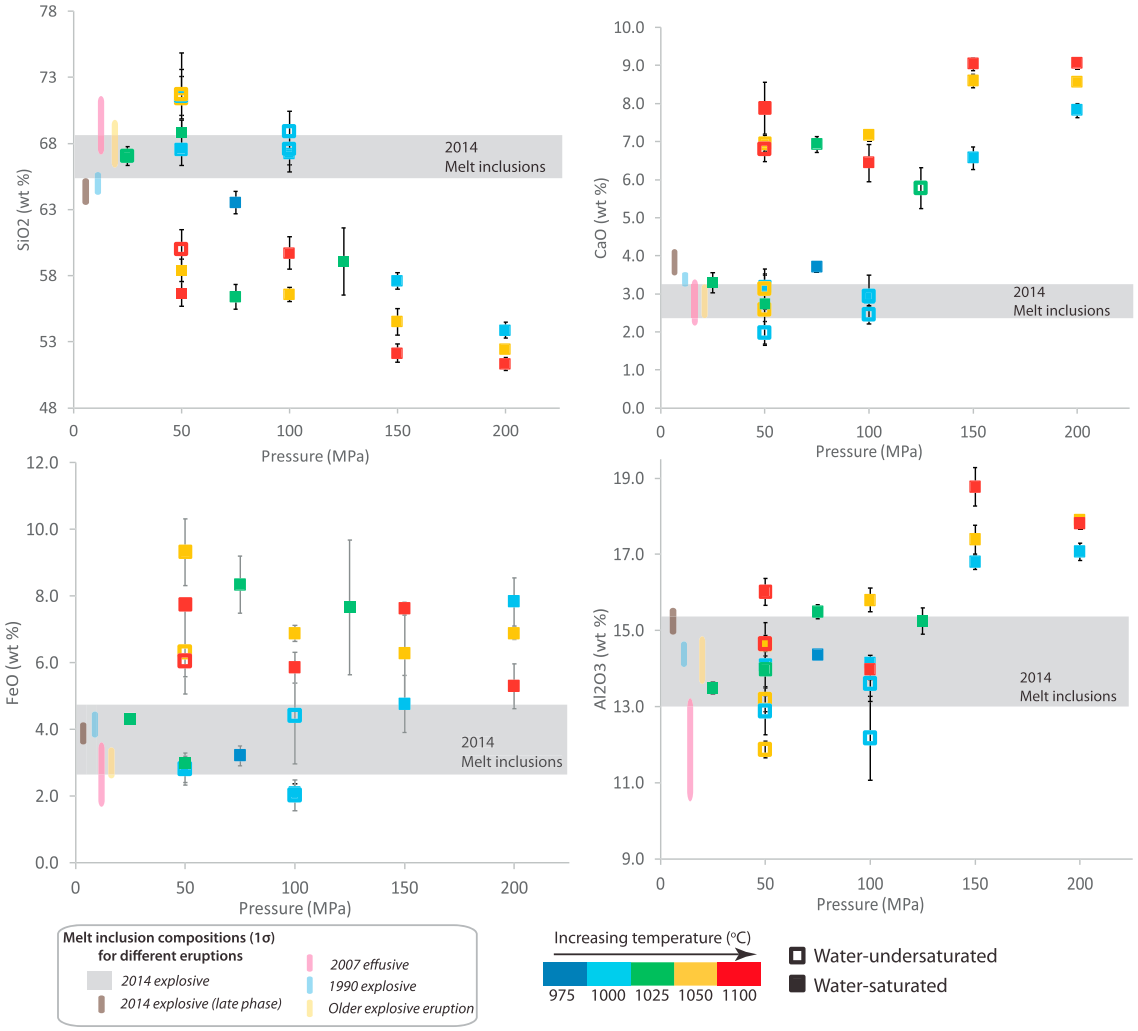

Figure 4. Dashed line/open symbol: where XH_2O is <1. Grey band = 1 standard deviation of melt inclusion composition. Error bar indicate 1 standard deviation of the glass data.

To match the experimental compositions with natural eruption products, melt inclusion compositions within nonantecrystic plagioclase phenocrysts were used as a representative composition of the preeruptive magma, while in storage, these had not crystallized, due to fast quenching and thus did not need to be corrected. This was preferred to matrix glass compositions, which can be affected by growth and nucleation of crystals upon ascent or cooling. To test this assumption, the 5% plagioclase microlite content (measured by image analysis) was subtracted from the matrix glass composition in a mass balance calculation. The microlite subtracted values closely resemble the average melt inclusion composition (<0.3 wt% difference for all elements; Table S2), confirming the melt inclusion composition is representative of the magma in storage. For the 2007 preeruptive composition, an averaged groundmass region (melt + crystals) was used due to the high proportion of crystallization within the melt inclusions and groundmass. In Figures 4 and 5, there is a general trend in glass compositions whereby experiments conducted at lower pressures, water contents, and temperatures generate more evolved compositions. This pattern extends to mineral compositions (Figure 6), where higher anorthite contents are stable at higher water pressures, whereas Mg numbers (Mg#) for clinopyroxene and orthopyroxene show a less discernible trend. All of the preeruptive glass and mineral compositions for the older explosive eruption, 1990, 2007, 2014, and late 2014 are reproduced with experiments at shallow pressures (25–100 MPa), temperatures between 975 and 1050 °C, and XH_2O values from 0.55 to 1 (Figures 4 and 6). However, specific compositional differences allow us to constrain this further for the individual eruptions of 2014 (main and late phase), 1990, 2007, and the older explosive eruption.

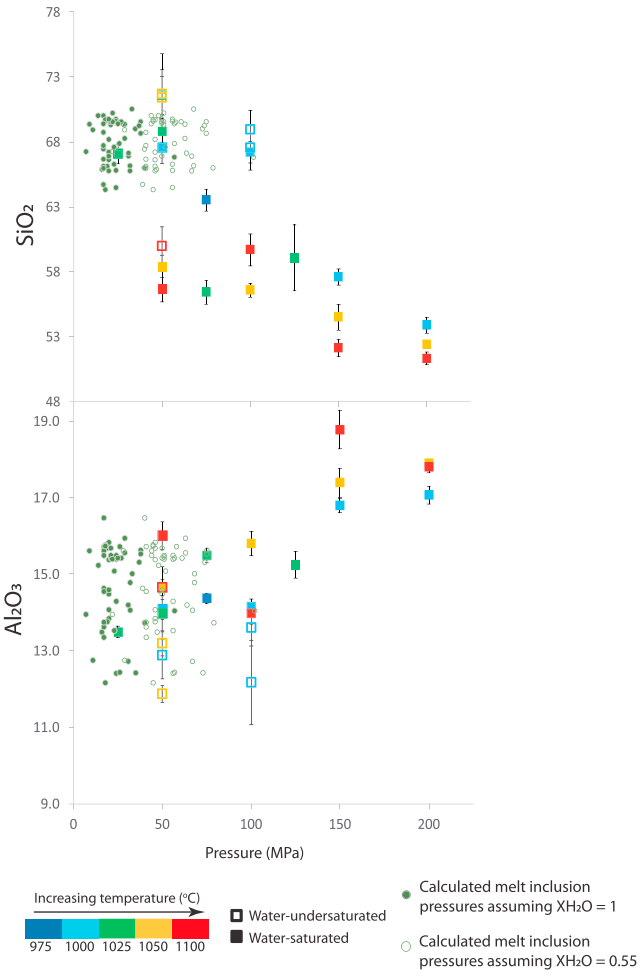

Figure 5. Experimental glass compositions with calculated water contents from solubility models (Papale et al., 2006) plotted on the same axis are melt inclusions and water contents measured via Raman spectroscopy from Cassidy et al. (2016).

For the main phase of the 2014 eruption (grey bars in Figures 4 and 6), the melt compositions are best reproduced across temperatures between 1000 and 1025 °C, which is particularly apparent in SiO_2 and FeO compositions. In addition, CaO, Al_2O_3, and orthopyroxene Mg# and anorthite show that the 2014 preeruptive compositions are best replicated by experiments conducted at water-saturated conditions. The glass chemistries appear to be more sensitive than mineral compositions to changing storage conditions. Pressures for the 2014 eruption can be constrained by using water content data measured in melt inclusions with Raman spectroscopy in Cassidy et al. (2016). Water contents extend to 2.2 wt%, which correspond to maximum storage pressure of 57 MPa (assuming water saturated conditions) or 102 MPa (assuming water undersaturated conditions, $XH_2O = 0.55$). The spread of water contents toward lower values (mean: 1.1 wt%) cannot be attributed to leaking or diffusion as this was assessed in Cassidy et al. (2016), and it is unlikely these melt inclusions were formed under storage pressures as low as 7 MPa (if water saturated). Instead, it suggests that the majority of these melt inclusions were entrapped when the magma was water undersaturated, this provides mean storage pressures of 52 MPa (at $XH_2O = 0.55$). Yet immediately prior to 2014 eruptions, these experiments show that the magma was water saturated. These P-T constraints are consistent with natural and experiment matches for An content of plagioclase (Figure 6a) and further by measurements made on feldspar phenocryst and glass contents as measured via EDS mapping (Figure 7). These constraints suggest the initial magma feeding the 2014 eruption was stored at temperatures of ~1000 ± 25 °C and 50–100 MPa, corresponding to a depth of ~1.9–3.8 km assuming a crustal density of 2,640 kg/m^3 (Smyth et al., 2007).

The old explosive eruption composition overlaps with the 2014 composition on most bulk and mineralogical chemical indicators and thus the same preeruptive constraints (1000 °C, 50–100 MPa, and $XH_2O = 1$) can also be applied to this unit. The 1990 and late 2014 products differ slightly in their preeruptive compositions, comprising lower SiO_2, (~3 wt%), and higher CaO contents (~0.5–1 wt%) than the 2014 melt compositions. Their preeruptive compositions overlap with experiments conducted at slightly deeper pressures (75 MPa—~3-km depth) and lower temperatures (975 °C) as shown in Figure 4, but these distinctions are more marginal and slight changes in the initial magma compositions may also account for this

The preeruptive composition of the 2007 (effusive) magma occupies a different chemical compositional space than the other eruptions (Figure 4), comprising higher SiO_2, lower Al_2O_3, and FeO glass contents and lower anorthite and Mg# in clinopyroxene (Figure 6). The 2007 preeruptive compositions therefore are better replicated by water undersaturated experiments ($XH_2O = 0.55$) at temperatures of 1000–1050 °C and pressures of 50–100 MPa (Figures 4 and 6). This corresponds well to the observation from the low water contents of Kelud melt inclusions (Figure 5), attributed to entrapment when the magma was in a water undersaturated state. These constraints from mineral and glass chemistry are further supported by glass and feldspar modalities, where the low glass contents and high phenocryst contents of the 2007 magma most closely match the, 50 MPa, 1000–1050 °C, water undersaturated experimental data.

3.3. Deformation Between December 2013 and May 2014

We do not detect any deformation in the period between 2 December 2013 and 8 February 2014, 3 days before the eruption (Figures 8a and S1). The small spatial footprint of CosmoSkyMed imagery combined with the lack of coherent points on Kelud's edifice mean that our measurements are sensitive to neither very deep (middless to lower crust >10 km) nor very shallow (<1 km) sources within the edifice itself. Given that

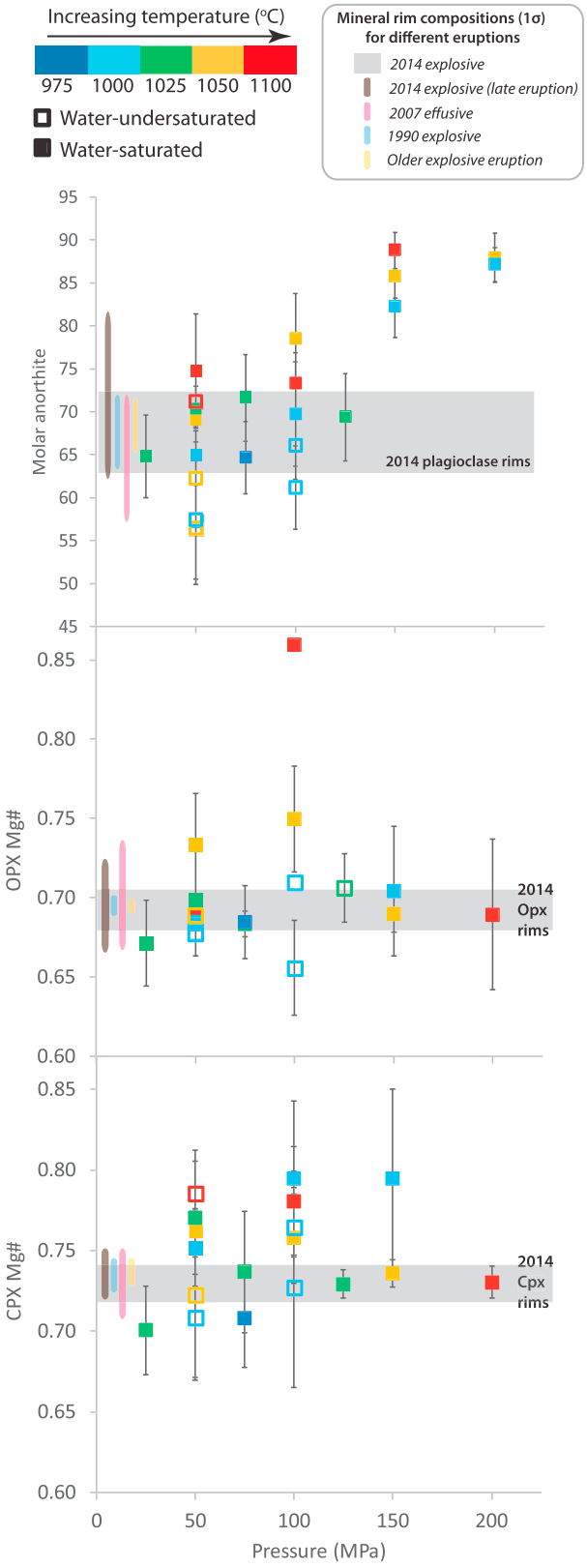

Figure 6. Mineral compositions of experimental samples compared to natural products Open symbols indicate mixed volatile conditions, where XH_2O = <1.

the preeruptive tilt is reported only at Kelud's crater and not at other stations further down the volcano's flanks (Nakamichi et al., 2017), it seems likely that its origin was shallow. This signal is centered within the zone of low phase coherence surrounding Kelud's summit and is likely to be well below detection thresholds at distances where InSAR measurement was possible. However, for a point source centered on the summit, we expect that larger volume changes >0.1 km^3 in the upper crust (e.g., depths up to <10 km) would be detectable.

In interferograms spanning the period between 8 and 20 February 2014 we observe an increase in line-of-sight (apparent displacement away from the satellite) around the southeastern rim of Kelud's edifice (Figure 8b shows time series solution for this period). This feature does not appear after 20 February. It is difficult to prove unequivocally that this is a real displacement rather than a phase delay due to differences in tropospheric water vapor. However, we note that this apparent subsidence is a consistent feature in the cumulative displacement time series for acquisitions dates after the eruption (Figures S1 and 8c). Since SAR satellites are side-looking, symmetrical subsummit deformation sources produce displacement signals that are both asymmetrical and off-center from the volcano summit in satellite line of sight (e.g., Magee et al., 2018). For the descending geometry of our CosmoSkyMed imagery (satellite heading = −168°, incidence angle = 32°), we expect a displacement signal that is offset from the summit toward the southeast for a centrally located geodectic source, which is consistent with our InSAR observations (Figure 8b).

We assume that any coeruptive, contracting deformation source is central (located within a few hundred metres of Kelud's summit crater) and uses a simple point-source model (Mogi, 1958) to make a first-order exploration of possible depths and volume changes. We perform a grid search of the parameter space between 0.5 and 15 km depth, -1×10^6 to -1×10^9 m^3 volume change and at locations at intervals of 50 m within 500 m of Kelud's crater. We find the lowest root mean square residuals for point sources close to the crater at depths of >~2 km could be consistent with the apparent coeruptive subsidence (an indicative source model located at (112.309°, −7.90°), 2.1-km depth, and -7×10^6 m^3 change in volume). However, we note that root mean square residuals of similar magnitude can also be obtained at greater depths (up to 7 km). Model solutions are nonunique, due to trade-offs between depths and volumes as well as because of the limited spatial coverage of our measurements. The assumption of a point-type source geometry may also be unrealistic, if, for example, pressure changes take place over a more vertically extensive ellipsoidal reservoir.

Given the limitations on our measurements, we restrict ourselves to the following, largely qualitative conclusions. First, that there was no deformation above our detection limits consistent with the intrusion of juvenile material between 2 December 2013 and 8 February 2014. Any preeruptive deformation was very shallow, originating within the volcano's edifice, as suggested by the near-vent tilt signals. Second, that the geodetic source for the coeruptive subsidence was below the edifice, resulting in a broader spatial footprint of deformation and subsidence in the more stably scattering areas where InSAR measurement is possible. We estimate the minimum depth for the source to be around 2 km, consistent with low

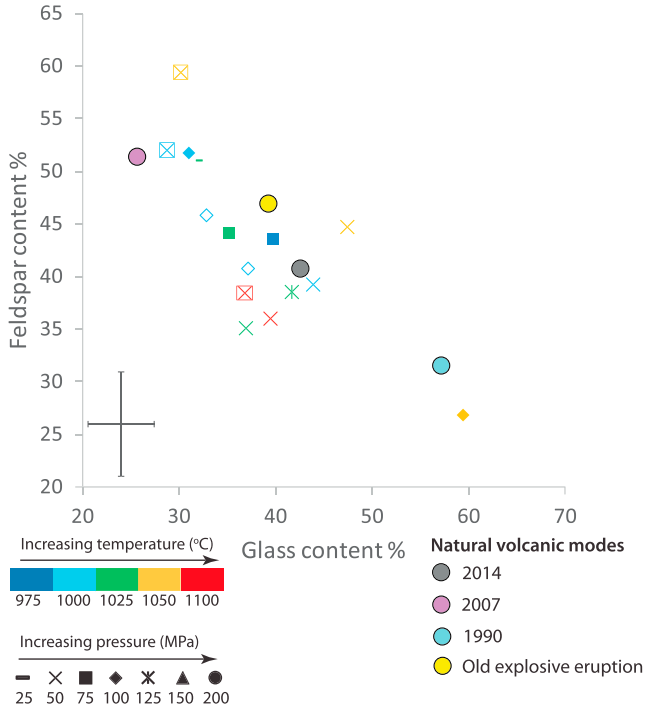

Figure 7. Glass and feldspar modes as calculated from energy dispersive spectrometer mapping images for selected experimental and natural samples. The use of glass here refers to the nonphenocrystic area for microlitic-rich groundmass samples such as 2007. Open symbols indicate mixed volatile conditions, where XH_2O = <1. Close matches between natural and experimental glass and mineral modalities further supports the storage P-T-XH_2O constraints from the chemical plots.

pressure estimates from experimental petrology (50 MPa), though it could also plausibly be deeper.

3.4. Timing From Seismicity and Infrasound Networks

Since the studies of Caudron et al. (2015) and Nakashima et al. (2016), additional seismic and infrasound data have been made available and processed. The broadband seismic data from the nearby Kawah Ijen volcano were analyzed in this study following the procedure described in Caudron et al. (2015). Figure 9 (upper panel) shows the seismic trace high-pass and low-pass filtered above 0.02 and below 0.1 Hz, respectively. Two signals separated by 15 min emerge in the spectrogram (Figure 9, lower panel). The results from a seismic antenna installed on the Merapi volcano and an infrasound array (Figure 10) located in Pelabuhan Ratu (West Java) are consistent with an acoustic origin for these two signals (Colbachini et al., 2016). These seismoacoustic signals likely correspond to (1) the initial phase of the eruption that destroyed the 2007–2008 dome plug and (2) the Plinian phase of the eruption that followed 15 min after.

3.5. Decompression Rates

Using image analysis of SEM images, the average bubble number density of the 2014 Kelud pumice comprised a volume (N_v) of 3,980 mm^{-3}, with a standard deviation of 862 mm^{-3} (n = 8, with a range of vesicularities). This value was then used in the equation of Toramaru (2006), which links nucleation theory to bubble number densities that are calibrated by decompression experiments, to calculate decompression rates for the 2014 Kelud eruption. Input values for the Toramaru (2006) decompression rate meter equation were provided from our experimental constraints, using temperatures of 1000 °C, water values of 2.48%, PSat of 50 MPa, and surface tension values from 0.02 to 0.05 N/m, as these values represent assumed heterogeneous bubble nucleation, consistent with the crystal-rich nature of the Kelud magma (Shea, 2017). This yields decompression rates of 0.1–0.12 MPa/s; this range is consistent with other explosive eruptions (Cassidy et al., 2018). It should be noted that decompression rates using bubble number densities most often record maximum rates, and not necessarily the average rates (Shea, 2017). Assuming a lithological gradient of 0.025 MPa/m, this equates to an ascent rate of 4–5 m/s. Using these ascent rates and the inferred crustal storage of 2–3 km, this gives a minimum time estimate of 7–12 min for the magma to ascend from storage.

4. Discussion

4.1. Shallow Preeruptive Storage of Crystal-Rich Basaltic Andesites

By matching experimental glass and mineral compositions, and mineral phase abundance with the natural eruptive products (Figures 4–7), we have been able to assess the preeruptive storage conditions for different eruptions at Kelud. The chemical and mineral characteristics of the 1990, 2007, and 2014, late phase 2014, and older explosive eruption can all be replicated with experiments at shallow pressures (25–100 MPa), temperatures between 975 and 1050 °C, and XH_2O values from 0.55 to 1 (Figures 4 and 6). These experimentally derived preeruptive storage constraints for the four different Kelud eruptions are compared to *P-T* estimates for other experiments conducted on intermediate magmas (Figure 11). This plot shows that preeruptive Kelud magmas are stored at temperatures comparable to other basaltic andesite magmas, but higher than commonly seen for andesites. The Kelud magmas however reside at shallower pressures (~<4-km depth) than all other basaltic andesite and andesite magmas, for which there are experimental data, but more akin to some shallow dacite magma reservoirs. One reason for this is that many experiments use fine powder or glass as opposed to the coarsely crushed sample used this and other studies (e.g., Erdmann et al., 2016). Therefore, in our experiments it was mostly dacitic compositions that were in equilibrium with the mineral phases; however, despite this, temperatures are generally much hotter than other dacites in this comparison.

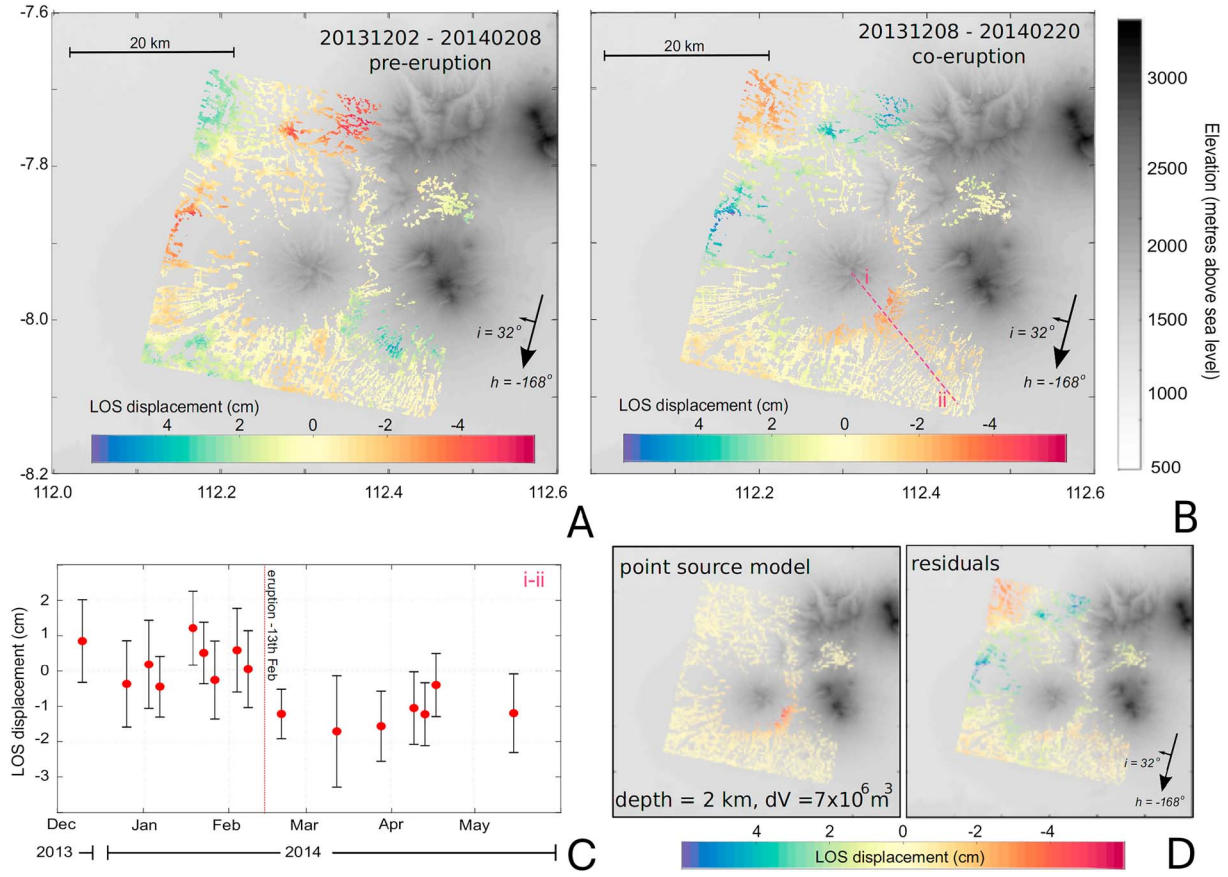

Figure 8. (a) Preeruptive line-of-sight displacement between 2 December 2013 and 8 February 2014, h = satellite heading, i = angle of incidence. (b) Coeruptive line-of-sight displacement between 8 and 20 February 2014. Note that the feature in the northwest quadrant of the image reverses in sign between panels (a) and (b) and is therefore likely to be an atmospheric feature associated with the image acquired on 8 February. (c) Time series showing the mean cumulative displacements for a wedge of $\pi/2$ centered on profile line *i*–*ii* and marked on panel (b). (c) Illustration of best, but not uniquely fitting, point source model (112.309°, −7.90°, 2.1-km depth, 7×10^6 m^3 loss of volume) and residuals.

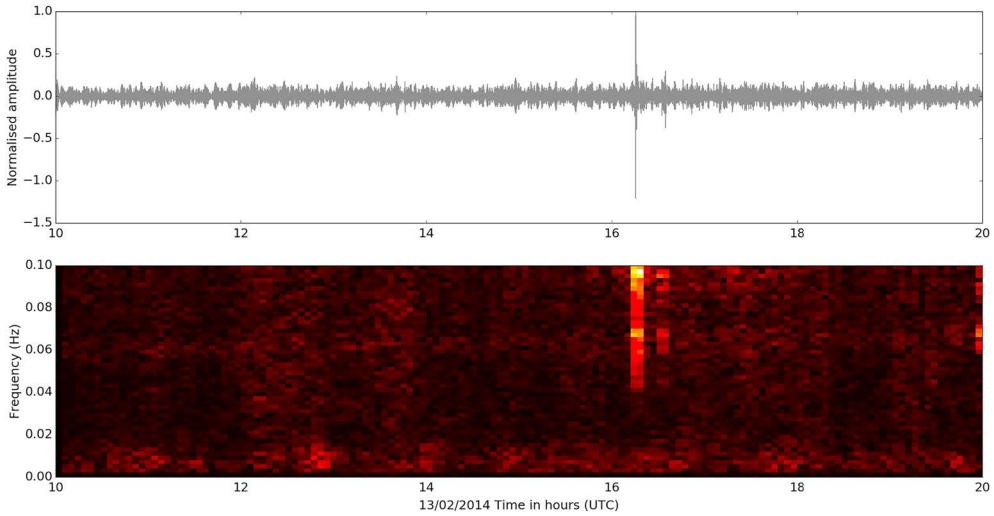

Figure 9. Upper panel: velocity waveform recorded by a broadband seismic station installed on the Kawah Ijen volcano (East Java, Indonesia) high-pass and low-pass filtered above 0.02 and 0.1 Hz, respectively. Lower panel: corresponding spectrogram computed using 500-s-long 1% cosine-tapered windows and showing two signals separated by ~15 min. The timing of wave arrival is consistent with the origin time and propagation velocities of the Kelud 2014 eruption presented in Caudron et al., 2015. Other causes of large seismic signals such as regional earthquake or teleseisms were also discarded.

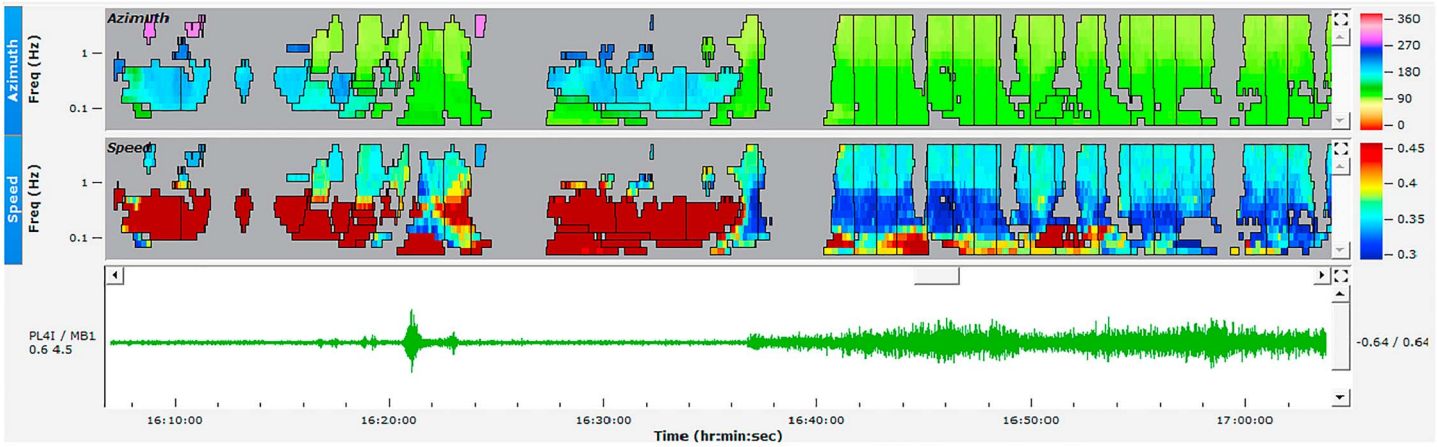

Figure 10. The upper and middle panels are time (*x* axis)-frequency (*y* axis) plots, with the colors corresponding to the azimuths (upper panel in degrees) and the speed (middle panel in m/s). Progressive Multi Channel Correlation (PMCC, Cansi, 1995; 15 log-spaced bands adapted from Matoza et al., 2013, and window lengths varying in proportion to the period from 30 to 250 s) results from the infrasound array installed in Pelabuhan Ratu (West Java) highlighting two clear signals starting at ~16:21 and 16:36 with an azimuth of ~90° pointing toward the Kelud volcano (upper panel) and typical acoustic speeds (~360 m/s, middle panel). The first signal is of short duration (a few minutes), while the second phase lasts for 2 hr (filtered between 0.1 and 5 Hz, lower panel).

It should be noted that the experiments conducted here replicate the last stage of shallow residence prior to ascent and eruption. Inevitably, the Kelud system will be fed from a deeper magmatic system, as evidenced by relict high anorthite cores in plagioclases and the presence of glomerocrysts, xenocrysts, and mineral-melt barometry (Cassidy et al., 2016; Jeffery et al., 2013).

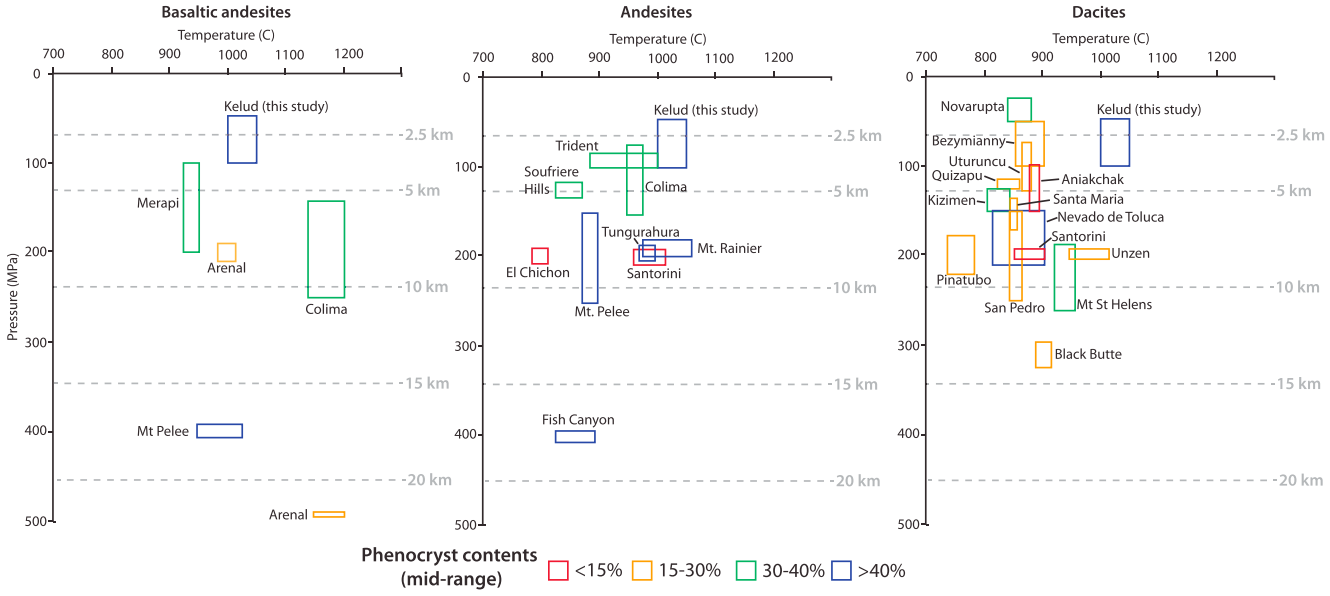

Figure 11. Comparison of preeruptive storage pressures and temperatures for other experiments (Joan Andújar et al., 2017) on intermediate magmas. Depth estimates from (left) Arenal (Parat et al., 2014; Pertermann & Lundstrom, 2006), Merapi (Erdmann et al., 2016), Shasta (Grove et al., 2003), Mt. Pelee (Martel et al., 1998; Pichavant et al., 2002). (middle) Basaltic andesites, Colima (Moore & Carmichael, 1998), Trident (Coombs et al., 2000), Soufrière Hills (Couch et al., 2003), El Chichón (Luhr, 1990), Mt. Rainier (Venezky & Rutherford, 1997), Santorini (Andújar et al., 2016). Tungurahura (Andújar et al., 2017), and Fish Canyon (Parat et al., 2008). (right) For Dacites; Nevado de Toluca (Arce et al., 2006, 2013), Novarupta (Coombs & Gardner, 2002; Hammer et al., 2002), San Pedro (Costa, 2004), Santorini (Cadoux et al., 2014), Mt St Helens (Rutherford & Devine, 1988), Aniakchak (Larsen, 2006), Black Butte (McCanta et al., 2007), Pinatubo (Scaillet & Evans, 1999), Unzen (Botcharnikov et al., 2008; Holtz et al., 2005), Santa Maria (Andrews, 2014), Fish Canyon (Caricchi & Blundy, 2015), Cerro Uturuncu (Muir et al., 2014), Kizimen (Browne et al., 2010), Bezymianny (Shcherbakov et al., 2013), Quizapu (First et al., 2017).

Such a low depth for preeruptive magmatic residence is more common for evolved magmas (such as dacites and rhyolites; e.g., Castro et al., 2013; Coombs & Gardner, 2002; Hammer et al., 2002), as magma will usually stall and accumulate in the parts of the crust where its density is the same as the surrounding rock, assuming there's no excess pressure, with crustal density normally becoming lower toward the surface (Lister & Kerr, 1991). However, there are some examples of dacitic magma storage stored at deeper depths (e.g., Mt St Helens, Black Butte and Mt Pintatubo) suggesting that this is not always the case (Figure 11). InSAR measurements of deformation, mostly in preeruptive periods, have been interpreted as evidence for shallow magma reservoirs (<3 km) at other Indonesian volcanoes, including Sinabung, Kerinici, Slamet, Lawu, Agung, and Anak Krakatau (Chaussard & Amelung, 2012).

The reasons behind Kelud's shallow magma storage are not entirely clear. Crustal heterogeneities, regional stress regime, local extensional fault networks, and Kelud's small edifice may all be important factors (Armienti et al., 2013; Castruccio et al., 2017; Pinel & Jaupart, 2000, 2004; Ten Brink & Brocher, 1987); however, this also may be partly due to Kelud's dichotomous composition and aided by the presence of exsolved volatiles. X-ray fluorescence data show that whole rock compositions for Kelud eruptive products plot consistently in the basaltic andesite field (Figure 3; 54 wt% SiO_2 average), whereas matrix glasses and melt inclusions are far more evolved (as their compositions have equilibrated in the shallow reservoir), plotting in the dacite field (67 wt% SiO_2 average; Figure 3). Therefore, it is perhaps the melt composition that defines the accumulation of magma at a certain depth rather than the crystals (or the combination), due to the enhanced mobility of melts relative to crystals, which promotes melt extraction and ascension. Deeper parts of the Kelud system have been proposed to be volatile rich (8 wt% water; Jeffery et al., 2013). Volatiles will exsolve during decompression and the retention of these exsolved volatiles (i.e., if the degassing system is closed) will also increase the overall buoyancy of the magma aiding shallow emplacement. As observed from previous studies at Kelud, the crystals have both grown within the magma during shallow residence, as evidenced by the evolved melt inclusion compositions and mineral-melt equilibrium (Cassidy et al., 2016), and some also have been brought up from deeper parts of the system as antecrysts, demonstrated by high anorthite plagioclase cores surrounded by less evolved rims grown within the shallow system (~10%; Jeffery et al., 2013). This suggests that the melt-rich magma does not simply ascend into an upper crystal mush, but that some of these antecrysts are “dragged up” with the magma and then grow and new crystals nucleate at shallower pressures during shallow level differentiation (e.g., Davidson et al., 2005). That Kelud magmas have had a consistent whole rock composition between different eruptions supports the notion that a common set of processes is continuously repeated at Kelud. Clearly not all of the magma in the reservoir will be erupted (e.g., 2007–2008 eruption at Kelud), and thus, there is mixing between old and new magmas, but trace element chemistry from mineral zoning suggests that recharging magmas have a similar chemical composition (Cassidy et al., 2016). The shallow storage of Kelud magmas may be a common feature of other crystal-rich and exsolved volatile-rich magmas with evolved melt compositions, a good example is Merapi volcano (Erdmann et al., 2016; Preece et al., 2013), which has very similar compositions and is also stored at shallow depths (Figure 11). More homogenous basaltic andesite magmas, where matrix glass and melt inclusions are also basaltic andesite, are stored at deeper depths (e.g., Arenal; Figure 11).| However, the color coding symbols according to phenocryst content (Figure 11) shows little relationship to magmatic storage depth.

Shallow (<3 km) geodetic sources have been observed in a range of volcanic settings, including in rift zones (e.g., Biggs et al., 2009, 2011), arcs (e.g., Chaussard & Amelung, 2012), and at ocean island volcanoes (e.g., Wolf, Sierra Negra, Galapagos, Bagnardi et al., 2013). However, many of these sources have been attributed to changes in hydrothermal systems and sill intrusions, rather than reservoir inflation, this illustrates the need to consider the presence of magma reservoirs at depths below 3 km.

4.2. Preeruptive Storage Conditions and Processes Prior to Explosive and Effusive Eruptions

We can constrain the preeruptive magmatic storage estimates of the individual eruptions based on their chemical comparisons with petrological experiments. The 2014, 1990, and old explosive eruption are most consistent with experiments conducted at 1000°± 25°C, 50–100 MPa, and $XH_2O = 1$ (water saturated). The 2007 effusive eruption was sourced from magmas under similar pressures (50–100 MPa), and temperatures (1000–1050 °C), but from a water-undersaturated (mixed with CO_2) magma ($XH_2O = 0.55$).

Cassidy et al. (2016) in a study of plagioclase phenocryst zoning highlighted the presence of temperature and water fluctuations during the evolution of magma in the reservoir. These temperature and water cycles were modulated by recharging magma that had higher temperatures and lower water contents, thus diluting the magmatic water content (e.g., 2007 effusive eruption). In the periods without magmatic recharge, the magma cooled and differentiated, driving up water contents (before the 2014 explosive eruption). The higher water contents coupled with increased viscosity (from cooling) was suggested to provide conditions that led to more explosive eruptions (Cassidy et al., 2016). This study reaffirms this hypothesis and shows that water contents (Figure 5), as measured by Raman spectroscopy in melt inclusions in Cassidy et al. (2016), may have been lowered in the effusive eruption by the presence of CO_2 in the fluid phase, which acted to supress water activity. Despite more CO_2 being present in the 2007 magmas ($XH_2O = 0.55$) and leading to lower water contents, little dissolved CO_2 is found in the melt inclusion compositions (<350 ppm), due to the low solubility of CO_2 at these shallow pressures, with the majority existing in the fluid/vapor phase (Moore, 2008; Papale et al., 2006). Our results suggest that Kelud magmas may spend the majority of their time in storage under water-undersaturated conditions (Figure 5) but may then become water saturated just before they erupt explosively.

The presence of months of midcrustal seismicity, elevated gas, increased lake temperatures, and higher estimated magmatic temperatures (Jeffery et al., 2013) prior to the 2007 effusive eruption, strongly point to a recharging system from intruding magma. The most notable signal of unrest was an increase of magmatic CO_2 emitted from the bottom of the crater lake four months prior to the eruption (Caudron et al., 2012). Given that the shallow reservoir (2–3 km) had likely degassed its CO_2, we suggest that this CO_2 outgassing is likely derived from deeper intruding magma, which diluted or suppressed the water contents in the shallow magma system (e.g., Cassidy et al., 2016). It is likely that the intrusion may have triggered the eruption, either via CO_2 outgassing (e.g., Caricchi et al., 2018) or simply the volumetric input of a degassed magma exceeding the yield strength of the overlying rocks (e.g., Degruyter et al., 2017).

Magmatic decompression rate (often coupled to ascent rate) is one of the strongest factors determining whether an eruption becomes effusive or explosive (Cassidy et al., 2018; Castro & Dingwell, 2009; Gonnermann & Manga, 2003; Jaupart & Allègre, 1991; Woods & Koyaguchi, 1994). The ascent of magma from depth is driven by the exsolution of volatiles into the vapor phase. When these exsolved volatiles remain coupled to the melt they increase the buoyancy of the magma and limit outgassing. Water as a magmatic volatile is particularly important for exsolution driven ascent as its solubility is such that it exsolves over a large pressure range of the magmatic system (Baker & Alletti, 2012; Petrelli et al., 2018). In contrast, the second most abundant volatile, CO_2, exsolves at deeper depths and thus is more likely to be lost before magmatic ascent occurs (Blundy et al., 2010). It is for this reason we suggest that magmas that are water saturated (and not just volatile saturated) prior to eruptions are more likely to be explosive (e.g., Stock et al., 2016). This hypothesis concurs with the estimates here for the ascent rates of the 2014 eruption of the Kelud magma (4–5 m/s), which are comparable to other explosive eruptions (Cassidy et al., 2018). The absence of deformation in the months before the 2014 eruption is consistent with a lack of a preeruptive intrusion of juvenile magma, at least after 2 December 2013 (earliest SAR image analyzed here). However, it is not diagnostic of there being no magma movement at all, as any intrusion may have been either too small to detect or to some extent accommodated by magma and reservoir compressibility, especially volatile-saturated magmas at shallow depths (high bubble fraction; e.g., McCormick-Kilbride et al., 2016).

4.3. Combining Petrology and Monitoring Data Sets to Track the Eruptive Progression

Using the multiparameter data collected in this study and others, we can piece together a likely series of events occurring prior, during and after the Kelud 2014 eruption. In the months leading up to the eruption there was little or no seismicity. Seismicity only started with small distal volcano-tectonic earthquakes a month prior, building up slowly, until shallow earthquakes (1–2 km) started occurring underneath the volcano itself some 2 weeks before (Nakamichi et al., 2017; Triastuty et al., 2014). Furthermore, in the 3-month period of satellite observation prior to the 13 February eruption, our study shows that there is no evidence of significant deformation in the coherent area surrounding the volcano's edifice. This suggests that no major volume changes were taking place in the crust at depths below ~2 km and is consistent with the lack of other signatures of magma injection before the 2014 eruption. This is in contrast to the evidence supporting magma intrusion as a trigger for the 2007 effusive eruption (e.g., 3 months of middle and upper crustal

seismicity, CO_2 degassing from the lake, higher estimated magma temperatures, mixed volatile conditions, and sieve texture and resorption zones within phenocrysts; Jeffery et al., 2013; Cassidy et al., 2016; Philibosian & Simons, 2011). The lack of a magma injection shortly before the 2014 eruption is consistent with phenocryst zoning signatures, which display normal zoning toward the rims of the feldspar crystals (Cassidy et al., 2016). The increased water contents in melt inclusions at the rims of feldspar crystals (Cassidy et al., 2016) and the water-saturated nature of the 2014 eruption from experiments suggest that volatile overpressure through differentiation and crystallization may be the most likely triggering mechanism (Blake, 1984; Fowler & Spera, 2008; Tait et al., 1989; Tramontano et al., 2017). The pronounced difference in magma water saturation between the 2007 and 2014 eruptions may be a consequence of the cooling and crystallization of the unerupted magma during or following the 2007–2008 eruption. This "internal" trigger or preconditioning for the 2014 eruption would also explain the lack of deep seismicity, widespread deformation and the short run-up times prior to the eruption. The volatile overpressure led to the initial eruption destroying the 2007–2008 dome and was followed by the main Plinian phase 15 min later (based on infrasound and seismic data presented here; Figures 9 and 10). This time lag corresponds closely with the estimates of ascent times calculated from bubble number densities from the pumices in the main Plinian stage. Decompression rates of 0.1–0.12 MPa/s (4–5 m/s) sourced from a magma at 50–100 MPa provide a minimum time estimate of 7–16 min for the magma to ascend from the reservoir. Therefore, the time lag between the two different eruptive phases implies rapid decompression of the Kelud magma reservoir immediately following the preliminary eruption as the cause for the high-intensity main Plinian phase of the eruption.

Between the main Plinian eruption and the waning stage, 2 hr later (Figures 10), the chemistry of the melt inclusions becomes less evolved (Figures 3). There is also a transition to more mafic compositions in the matrix glass and therefore after melt inclusion entrapment. This suggests that the eruption mixed with a likely deeper (or melt with different degrees of water saturation), more mafic reservoir as the magma tapped different melt bodies as a consequence of downward propagating decompression-driven eruption; e.g., Tarasewicz et al., 2012). This petrological finding could be consistent with the coeruptive subsidence signature detected to the southeast of the edifice (Figure 8b). This adds further complexity and unpredictability to the evolution of eruptions and how we monitor them.

4.4. Is Magmatic Ascent Related to the Onset of Unrest?

Unrest detected via monitoring techniques is commonly linked to ascent of magma through the crust (Sparks, 2003; Sparks et al., 2012), or even from magma chamber to surface (Passarelli & Brodsky, 2012). However, recent studies suggest that nonmagmatic unrest is common and unrest is not always associated with 'magma on the move' (Pritchard et al., 2019). Figure 12 agrees with the latter view and shows that the final ascent/decompression from a preeruptive magma reservoir can occur very rapidly in explosive eruptions, even when sourced from deeper reservoirs (>7 km). Furthermore, this ascent time is often decoupled from the onset time of unrest, as in the case for Kelud (Figure 12). The time of magmatic ascent for various explosive and effusive eruptions in Figure 12 has been calculated from the ascent rate compilation from Cassidy et al. (2018), and preeruptive storage depth estimates for the individual eruptions were taken from the literature. When known, the onset of unrest time is plotted for the same eruptions using the Global Volcanism Program reports. We use the term "onset of unrest" to describe the time at which the background/baseline behavior of a volcano increases sufficiently to be notable and reported (akin to Phillipson et al., 2013). Figure 12 shows that due to the difference in ascent rates, magmas feeding effusive eruptions take longer to ascend (days to years), compared to explosive eruptions (minutes to days), but there is some overlap. Some eruptions, all of which are effusive, have onset of unrest times close to the estimated magma ascent time (e.g., Soufriere Hills, Colima 1998, and Mt. St. Helens), an observation that is consistent in these cases with unrest being a direct reflection of magma ascent from the uppermost reservoir. However, other dominantly effusive eruptions have longer time gaps between the onset of unrest and their estimated ascent time (e.g., 1991 Unzen and 2011 Cordon Caulle). A caveat here is that magma may sometimes travel long distances laterally before erupting (e.g., Castro et al., 2013; Jay et al., 2014). Equally likely is that magma starts to move at the onset of unrest, but it stalls because of unfavorable thermal or stress conditions, which can lengthen unrest timescales, particularly for volcanoes that have not erupted for a long time period (Pritchard et al., 2019). In such instances the ascent time or rate as calculated from depth is not

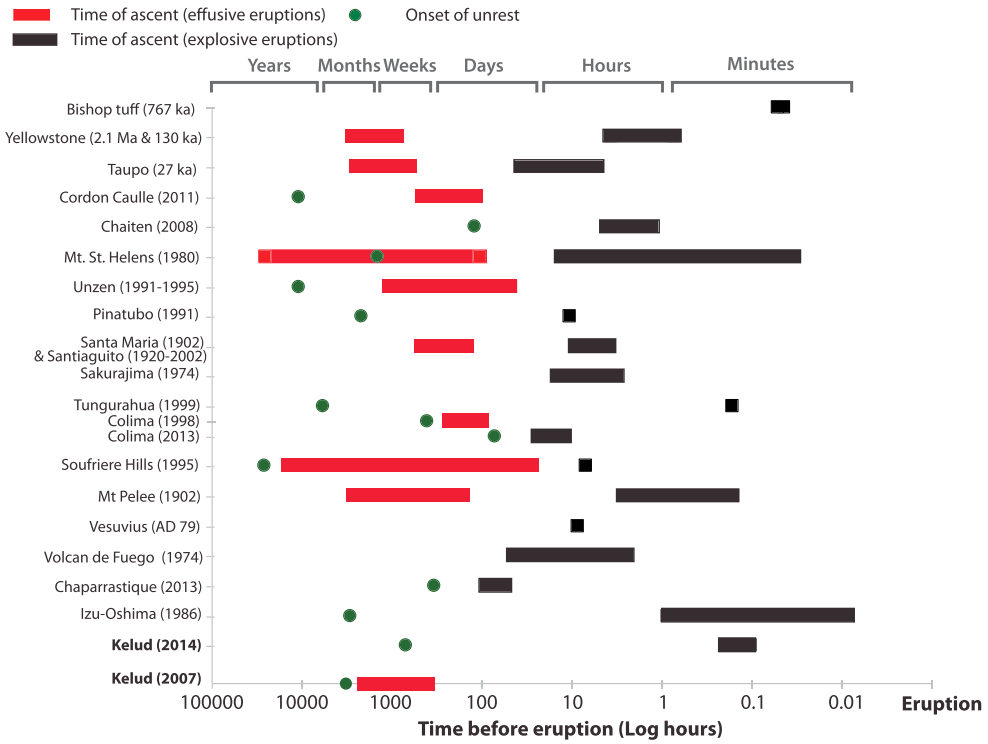

Figure 12. Ascent and run up timings for explosive and effusive eruptions, with known ascent rates, storage depths, and unrest timescales. Where onset of unrest times are not known, the ascent time estimates are plotted for comparison. It should be noted that not all eruptions were exclusively explosive or effusive, for example, Cordon Caulle; however, we defined them by their dominant eruptive style. Ascent rates are from the compilation of Cassidy et al. (2018), depth estimates from Izu-Oshima, Japan (Hamada et al., 2014), Chaparrastique, El Salvador (Scarlato et al., 2017), Arenal, Cost Rica (Parat et al., 2014), Vesuvius, Italy (Scaillet et al., 2008), Mt Pelee (Martel et al., 1998), Soufriere Hills, Montserrat (Barclay et al., 1998), Colima, Mexico (Moore & Carmichael, 1998), Tungurahua, Ecuador (Andújar et al., 2017), Sakurajima, Japan (Miwa et al., 2009), Pinatubo, Philippines (Rutherford & Devinel, 1996), Santiaguito, Guatemala (Scott et al., 2012), Santa Maria, Guatemala (Andrews, 2014), Unzen, Japan (Holtz et al., 2005), Mt. St. Helens (Rutherford & Devine, 1988), Chaiten, Chile (Castro & Dingwell, 2009), Taupo, New Zealand (Smith et al., 2005), Yellowstone, United States (Myers et al., 2016), and Bishop Tuff, United States (Wallace et al., 1999).

appropriate. In contrast to the effusive examples, all of the compiled explosive eruptions have ascent times orders of magnitude shorter than the first signs of unrest (even when this unrest period is itself relatively short). We therefore infer that unrest signatures in these cases are mostly unrelated to magmatic ascent to the surface. Instead, these signatures from seismicity or in other forms may either be related to magmatic movement deeper in the plumbing system, "fluids on the move" or could be linked to stress changes on faults, aquifers and hydrothermal systems (e.g., White & McCausland, 2016).

One of the big caveats here is the use of syneruptive ascent rates to compare with preeruptive unrest, as some magmas may have ascended slowly prior to eruption and rates then increased once the eruption began during rapid decompression (e.g., Mt St Helens cryptodome, 0.01 m/s; Endo et al., 1981). This two-stage process would lengthen the ascent time. Another caveat, however, may make the ascent times shorter than plotted. Here, we have assumed magmastatic pressure equals lithostatic pressure, which may not be the case for overpressured systems. For example, if maximum magmatic overpressures of 20 MPa were assumed (Sparks, 1997), this would equate to a ~0.77 km reduction in estimated depths, which would make the ascent times slightly shorter than plotted for overpressurized systems.

Figure 13 plots some of the variables used to calculate ascent times in Figure 12 against each other. This shows that most eruptions are sourced from reservoirs from 4 to 9 km, with no discernible difference between effusive and explosive eruptions, suggesting that storage pressure (and by extension dissolved volatile contents) ultimately have little control on eruptive style, as we have found for the Kelud system. Kelud's shallow storage depth may have added to the lack of prewarning, as magma is ascending for a

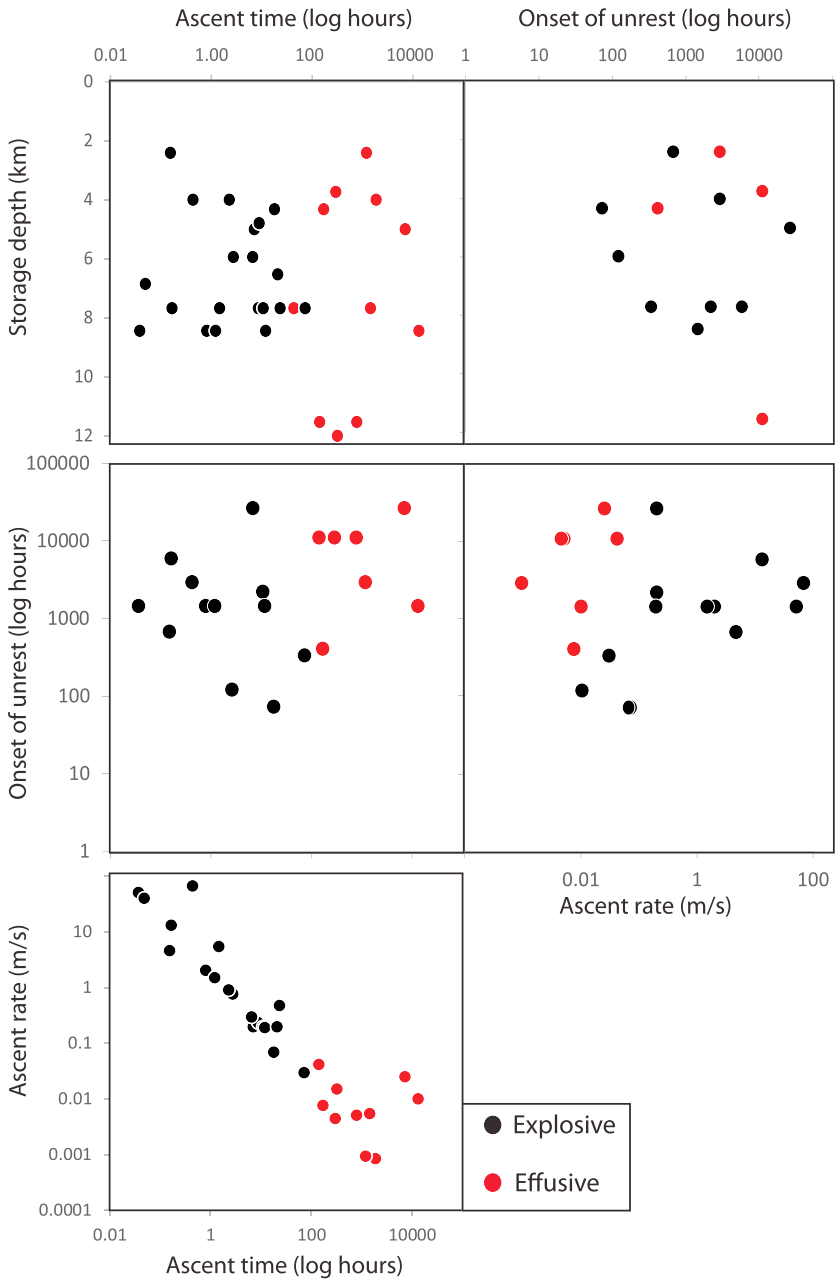

Figure 13. Plots comparing storage depths, onset and unrest timescales to ascent time, and rates for both explosive (black symbols) and effusive eruptions (red symbols).

shorter time period relative to magmas stored deeper. However, when plotting ascent time versus preeruptive storage depth (Figure 13a), there is no significant correlation, despite the fact that the ascent time was calculated partly from storage depth. Instead, it shows that ascent time is most dependent on the rate of ascent (Figure 13e). Figures 13c and 13d show that the onsets of unrest are not correlated with ascent times or rates. However, for the eruptions where the time of onset is longest, the ascent time is also the longest (along with slower ascent rates). These plots also show that effusive eruptions generally have longer periods of unrest (effusive mean is 380 days, explosive mean is 226 days), a slower magma ascent rate and this magma takes longer to ascend (mean ascent effusive time is 98 days, with explosive eruptions averaging 10 hours), which has implications for forecasting the eruptive style of an impending eruption.

4.5. Explosive Eruptions With Little Warning

Prior to the 2014 VEI our explosive eruption, Kelud showed limited evidence for major deformation up to three months prior. Seismicity was low, shallow, and accelerated quickly 10 days prior to the eruption, such that failure forecast modeling, conducted retrospectively, could not predict the start of the eruption, estimating it 3 days to 2 weeks late (Nakamichi et al., 2017). This rapid ramp-up of activity prior to an explosive eruption is particularly hazardous, requiring fast decision making and evacuations to take place, which in the case of Kelud was conducted successfully 2 days before the eruption, leading to limited causalities (Venzke, 2018). To understand the lead-up of unrest prior to other explosive eruptions, we have compiled a list of all the VEI $\geq$4 eruptions since 1992 (when satellite measurements of deformation began) from the literature (Table S3 and Figure 14). Here, we use onset of any volcano-related seismicity as described in the particular publication or the Global Volcanism Program reports (Table S3). Distal VT seismicity, defined in White and McCausland (2016) as "high-frequency volcano tectonic earthquakes at distal locations on tectonic fault structures at distances of one or two to tens of kilometers laterally from the site of the eventual eruption," is provided by Table 1 in White and McCausland (2016). Out of the 22 eruptions, no measurements were made on three eruptions and some had limited information or uncertainty in the monitoring data (Figure 14). Nevertheless, this data set shows that more than a third of VEI 4+ eruptions since 1992 occurred with less than 2 weeks notice and over a half (52%) occurred within only a month of the first sign of unrest. It should be noted though that for some eruptions, given a more developed monitoring network, more subtle unrest activity (e.g., distal VT seismicity) might have identified unrest further in advance. There is a large range in the preeruptive unrest time periods, ranging from a few hours before an eruption (Calbuco, 2015) to deformation over decade-long intereruptive periods at Okmok (2008). Also plotted in Figure 14 are the type of unrest signals, being seismicity, distal VT seismicity, deformation measured by InSAR and via tilt or GPS, and phreatic or fumerolic activity. In 8 of 19 eruptions, some form of deformation (inflation or deflation, measured either in situ or remotely sensed) was the first sign of unrest, often occurring months to years prior to an eruption, and even months to years prior to any other sign of unrest. Indeed, some preeruptive periods show long-term changes in deformation, but only a short run-up of seismic activity (e.g., Okmok, Grimsvotn, and Wolf). Deformation can be caused by a range of volcanic processes including magma movement, degassing and phase changes, and hydrothermal processes (e.g., Biggs et al., 2014; Ebmeier et al., 2018; Hamlyn et al., 2018; Pinel et al., 2014). Even if deformation can be confidently attributed to magma movement, this is not necessarily a sign of imminent eruption, and more detections of deformation have been made during unrest than can be clearly linked to periods of eruption (e.g., Biggs et al., 2014; Ebmeier et al., 2018; Jay et al., 2014). Bodies of magma can build up gradually by a process of successive intrusions (e.g., Santorini, Parks et al., 2012; Pyle, 2017) or by posteruption recharge (e.g., Okmok, Lu & Dzurisin, 2014) and reside in the crust for months to decades before eruption. On a multidecadal time scale, detection of deformation is a good statistical predictor for an eruption taking place over the same period of observation (Biggs et al., 2014; Furtney et al., 2018). However, eruptions have also taken place at volcanoes where a lack of deformation has been measured (Rasmussen et al., 2018). At Kelud a shallow magma body (at 2–4 km) may have resided undetected until it was triggered shortly before the eruption in 2014, which has parallels in other eruptions with only short periods of preeruptive seismicity (Reventador, Rabaul 1994, Kasatochi, Calbuco, Chaiten, Manam, and Ruang).

The rapid onset of unrest prior to the Reventador 2002 eruption was attributed to its low silica, volatile-rich, fluid magma, making it ascend aseismically (Hall et al., 2004). Stix (2018) also suggests "fast" volcanoes, those with onset of unrest times of months to years prior, are derived from volatile-rich, mobile magma, with fast ascent rates, whereas "slow" volcanoes, those displaying restlessness over the course of decades have complex plumbing systems, erupted magmas that are partly degassed and rheologically sluggish. Absolute volatile contents or magma water contents are difficult parameters to compare, as these relate to the solubility limit and therefore the depth at which the magma resides, making magma water content comparisons meaningless unless corrected for depth, and we show here that magma storage depth has little effect on onset time and eruptive style (Figure 13). The data presented here show that high-silica and high-viscosity magmas can also erupt with little warning and that when ascent times for explosive eruptions are on the order of minutes to days, then ascent does not need to be aseismic, but simply rapid without much prior magma movement required. Data from White and McCausland (2016) now show that distal VTs were recorded up to a month before the 2002 Reventador eruption,

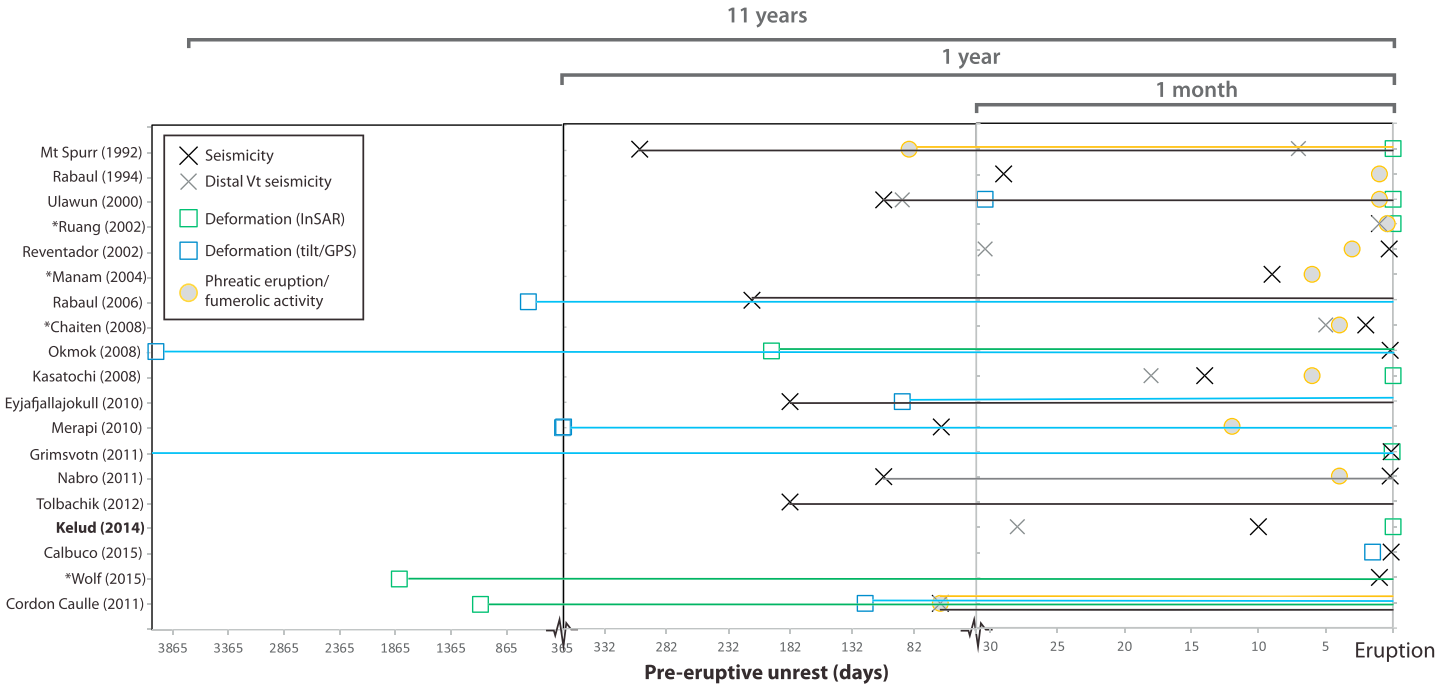

Figure 14. Run-up time for explosive eruptions VEI 4 and greater since 1992. The eruptions of Lascar (1993), Sheveluch (1999) and Sarychev Peak (2009) were not included due to insufficient monitoring data collected. The symbols indicate the onset of unrest, and the colored lines denote unrest that was recorded >1 month prior to the eruption. The color indicates the type of unrest signal, in accordance with the symbol colors. The symbol "*" indicates eruptions with patchy monitoring data sets, and thus, there is uncertainty over run-up times. Data compiled for this figure is from Global volcanism reports (ed. Venzke, 2018), distal seismic data from White and McCausland, (2016), and the following sources: Cordon Caulle, (Jay et al., 2014); Wolf (de Novellis et al., 2017; Xu et al., 2016); Calbuco (Delgado et al., 2017); Kelud (Nakamichi et al., 2017); Tolbachik (Lundgren et al., 2015); Nabro (Goitom et al., 2015; Hamiel & Baer, 2016; Hamlyn et al., 2014); Grimsvotn (Bato et al., 2016; Hreinsdóttir et al., 2014; Reverso et al., 2014); Merapi (Costa et al., 2013; Pallister et al., 2013; Saepuloh et al., 2010); Eyjafjallajokull (Sigmundsson et al., 2010), Kasatochi (Ruppert et al., 2011; Waythomas et al., 2010); Okmok (Freymueller & Kaufman, 2010; Lu et al., 2010; Passarelli & Brodsky, 2012); Chaiten (Wicks et al., 2011); Rabaul (Bouvet de Maisonneuve, 2015); Manam (Global Volcanism Program, 2004); Reventador (Hall et al., 2004); Ruang (Bebbington & Marzocchi, 2011; Marzocchi & Bebbington, 2012; Phillipson et al., 2013; Wunderman, 2002); Ulawun (White & McCausland, 2016; Wunderman, 2000); and Rabaul (Bouvet de Maisonneuve, 2015; Venzke, 2013); Mt Spurr (Gardner et al., 1998; Phillipson et al., 2013; Power et al., 2002; Wiemer & McNutt, 1997). A compiled data table can be found in the supporting information.

but not recognized at the time as being associated with volcanic unrest at Reventador volcano as these are likely related to stress changes on peripheral faults and aquifers resulting from the pressurization of the magma reservoir. These distal VTs could be important for forecasting rapid onset explosive eruptions, as they often occur earlier than other forms of seismicity (e.g., Nabro, Kelud, Kasatochi, and Reventador; Figure 14) or unrest signatures, and their magnitudes may be related to intruded volumes (White & McCausland, 2016).

Some eruptions on Figure 14 are preceded by longer periods of unrest and display multiple unrest signals that initiate at similar times (e.g., Cordon Caulle, Eyjafjallajokull, and Ulawun). Where this happens, deformation signals (when caused by magma) may more likely be related to magma injections that trigger ascent and eruption (e.g., Rasmussen et al., 2018). Indeed, timescales of magmatic injection prior to eruptions gained from diffusion chronometry, often provide estimates on the order of months to decades (e.g., Bouvet de Maisonneuve, 2015; Druitt et al., 2012; Till et al., 2015). Above, we attribute the limited uplift signatures and rapid onset seismicity before the 2014 Kelud eruption and others to internal triggering via volatile saturation. We therefore propose that the different unrest time signatures may be attributed to the manner with which the eruptions were triggered. The eruptions that have longer periods of unrest of different types occurring at similar times may be associated with a magmatic injection trigger generating seismicity as the magma ascends and causes uplift and inflation of the edifice. In contrast, the eruptions with a more rapid onset of seismicity prior to the eruption (or decoupled from the deformation signature) may be triggered internally, not requiring fresh inputs of magmas but resulting from a magma crystallizing as it cools (second boiling). This leads to volatile saturation and high overpressures, likely leading to faster

magma ascent; indeed, a recent study by Tramontano et al. (2017) shows that shallow reservoirs (<11 km) are more susceptible to be triggered by volatile overpressure. These conditions shorten the onset of unrest, make explosive eruptions more likely, and lessen the likelihood of detecting precursory activity. A complexity to this argument is that magmas can undergo several different processes prior to eruptions, such as magmatic injections which albeit do not trigger the eruption directly, but may precondition the magma making it more susceptible to final triggering by some other later process, such as second boiling, as was the case for Kelud.

5. Conclusions

By combining experimental and analytical petrology with monitoring and satellite data, we have been able to deduce the following:

1. Preeruptive basaltic andesite magmas for various different eruptions at Kelud are stored at temperatures of 1000–1050 °C and low pressures (50–100 MPa) equating to depths of 2–4 km. These storage depths are shallower than other basaltic andesite or even andesite magmas but are more akin to more silicic magmas. We speculate that this shallow storage may be related to Kelud's exsolved volatile- and crystal-rich magma with a more evolved melt composition. Kelud magmas are mixtures of silicic melt and mafic crystals and thus different from pure basaltic andesites melts, and as a result can reach neutral buoyancy within the crust and carrying its accompanying crystals.
2. The biggest difference in preeruptive storage conditions between eruptions is the range of water fractions (XH_2O), which ranges from water saturated in the explosive eruptions to water undersaturated conditions (those mixed with CO_2; $XH_2O = 0.55$) in the 2007–2008 effusive eruption. This effusive eruption was likely triggered by a CO_2-rich magma injection that heated the magma and suppressed its water contents. We attribute the greater explosivity of the 2014 eruption to its water-saturated nature. Water has a large exsolution pressure range which aids buoyancy and fast ascent, relative to CO_2, which is often degassed at shallow pressures and can decouple from the melt.
3. The limited amount of unrest and deformation prior to the 2014 explosive eruption, combined with its water-saturated nature, suggests that volatile overpressure triggered the eruption (internally triggered). The initial phase of the eruption destroyed the 2007–2008 dome plug and led to rapid decompression of the underlying shallow magma reservoir producing a high Plinian plume 15 min later, a time lag gained from infrasound and seismic data, but one that is also consistent with calculated decompression rates from bubble number densities. Several hours following the main Plinian phase, the eruption energy waned, leading to a low altitude plume distributing ash to the northeast regions. The ash from this phase of the eruption comprised less evolved melt inclusion and matrix glass compositions, evidence that points to the tapping of deeper and more mafic magma bodies during the eruption. Coeruptive subsidence from our InSAR data could be caused by geodetic sources at depths of 2–7 km. These combined petrological and geodetic observations suggest deeper melts were tapped as the eruption progressed, sustaining the Plinian eruption.
4. Compilations of calculated ascent times and onsets of unrest periods for multiple explosive and effusive eruptions at other volcanoes show that there is often a large gap between the onset of unrest and the ascent time of the magmas, highlighting that unrest signatures rarely correspond to direct magma ascent to the surface. We find that effusive eruptions have longer preeruptive unrest periods as well as longer ascent times, but that explosive eruptions can ascend in a matter of minutes to hours even when sourced from deep reservoirs. Magmatic depth does not seem to affect whether eruptions are explosive or effusive, as in the Kelud example, and ascent time is mostly controlled by ascent rate rather than the depth at which magma is stored.
5. In a compilation of onset of unrest times for all VEI 4 eruptions since 1992, we find that over a half occur with only a month or less of unrest prior to erupting. For others, deformation signals can occur for months or years before an eruption, but some eruptions show limited deformation in the months prior to an eruption if they are not triggered by magmatic injections. We show that compositional differences related to viscosity have no bearing on ascent times or the duration of preeruptive unrest. Using results from the Kelud 2014 eruption, we propose that explosive eruptions with little warning are mostly triggered internally, via volatile saturation and overpressure, rather than externally (i.e., by magma injection).

Acknowledgments

COSMO-SkyMed imagery were obtained through a UK Satellite Applications Catapult COSMO-SkyMed Radar Science and Innovation Research (CORSAIR) project. The TanDEM-X WorldDEM used for topographic corrections was provided through a TanDEM-X Science Proposal (DEM_GEOL1333). Some of the EMPA analyses costs were covered by a NERC-COMET small grant to S. K. E., M. C., and S. F. L. W. S. K. E. is supported by a Leverhulme Early Career Fellowship and by the European Space Agency's Living Planet fellowship programme. M. C. acknowledges an Alexander Von Humboldt fellowship and a NERC Independent Research fellowship, NE/N014286/1. We thank Rémi Colbalchini, Jean-Philippe Métaxian, Thibault Arnal, and Alexis Le Pichon who constructed the Figure 10 and shared their insights into seismo-acoustic data from Pelabuhan Ratu and Merapi volcano. Thanks also to Stephan Buhre for EMPA assistance. The experimental work was supported in part by the VAMOS research center at the Johannes Gutenberg University of Mainz, Germany. We thank Tom Shea and two anonymous reviewers for their helpful feedback to improve this paper. Data for this paper can be accessed through National Geoscience Data Centre (NGDC): https://www.bgs.ac.uk/services/NGDC

References

Alidibirov, M., & Dingwell, D. B. (1996). Magma fragmentation by rapid decompression. *Nature*, *380*(6570), 146–148. https://doi.org/10.1038/380146a0

Andrews, B. J. (2014). Magmatic storage conditions, decompression rate, and incipient caldera collapse of the 1902 eruption of Santa Maria Volcano, Guatemala. *Journal of Volcanology and Geothermal Research*, *282*, 103–114. https://doi.org/10.1016/j.jvolgeores.2014.06.009

Andújar, J., Scaillet, B., Pichavant, M., & Druitt, T. H. (2016). Generation conditions of dacite and rhyodacite via the crystallization of an Andesitic magma. Implications for the plumbing system at Santorini (Greece) and the origin of tholeiitic or calc-alkaline differentiation trends in arc magmas. *Journal of Petrology*, *57*(10), 1887–1920. https://doi.org/10.1093/petrology/egw061

Andújar, J., Martel, C., Pichavant, M., Samaniego, P., Scaillet, B., & Molina, I. (2017). Structure of the plumbing system at Tungurahua volcano, Ecuador: Insights from phase equilibrium experiments on july-august 2006 eruption products. *Journal of Petrology*, *58*(7), 1249–1278. https://doi.org/10.1093/petrology/egx054

Andújar, J., & Scaillet, B. (2012). Experimental constraints on parameters controlling the difference in the eruptive dynamics of phonolitic magmas: The case of tenerife (Canary Islands). *Journal of Petrology*, *53*(9), 1777–1806. https://doi.org/10.1093/petrology/egs033

Annen, C., Blundy, J. D., & Sparks, R. S. J. (2006). The genesis of intermediate and silicic magmas in deep crustal hot zones. *Journal of Petrology*, *47*(3), 505–539. https://doi.org/10.1093/petrology/egi084

Arce, J. L., Gardner, J. E., & MacÍas, J. L. (2013). Preeruptive conditions of dacitic magma erupted during the 21.7 ka Plinian event at Nevado de Toluca volcano, Central Mexico. *Journal of Volcanology and Geothermal Research*, *249*, 49–65. https://doi.org/10.1016/j.jvolgeores.2012.09.012

Arce, J. L., Macias, J. L., Gardiner, J. E., & Layer, P. W. (2006). A 2.5 ka History of dacitic magmatism at Nevado de Toluca, Mexico: Petrological, $^{40}Ar/^{39}Ar$ dating, and experimental constraints on petrogenesis. *Journal of Petrology*, *47*(3), 457–479. https://doi.org/10.1093/petrology/egi082

Armienti, P., Perinelli, C., & Putirka, K. D. (2013). A new model to estimate deep-level magma ascent rates, with applications to Mt. Etna (Sicily, Italy). *Journal of Petrology*, *54*(4), 795–813. https://doi.org/10.1093/petrology/egs085

Bachmann, O., & Bergantz, G. (2008). The magma reservoirs that feed supereruptions. *Elements*, *4*(1), 17–21. https://doi.org/10.2113/GSELEMENTS.4.1.17

Badrudin, M. (1994). Kelut volcano monitoring: Hazards, mitigation and changes in water chemistry prior to the 1990 eruption. *Geochemical Journal*, *28*(3), 233–241. https://doi.org/10.2343/geochemj.28.233

Bagnardi, M., Amelung, F., & Poland, M. P. (2013). A new model for the growth of basaltic shields based on deformation of Fernandina volcano, Galápagos Islands. *Earth and Planetary Science Letters*, *377-378*, 358–366. https://doi.org/10.1016/J.EPSL.2013.07.016

Baker, D. R., & Alletti, M. (2012). Fluid saturation and volatile partitioning between melts and hydrous fluids in crustal magmatic systems: The contribution of experimental measurements and solubility models. *Earth-Science Reviews*, *114*(3-4), 195–217. https://doi.org/10.1016/j.earscirev.2012.06.002

Barclay, J., Rutherford, M. J., Carroll, M. R., Murphy, M. D., Devine, J. D., Gardner, J., & Sparks, R. S. J. (1998). Experimental phase equilibria constraints on preeruptive storage conditions of the Soufriere Hills magma. *Geophysical Research Letters*, *25*(18), 3437–3440. https://doi.org/10.1029/98GL00856

Bato, M. G., Pinel, V., & Yan, Y. (2016). Volcano deformation and eruption forecasting using data assimilation: Building the strategy. *American Geophysical Union, Fall Meeting 2016,* Abstract #G23A-1028. Retrieved from http://adsabs.harvard.edu/abs/2016AGUFM.G23A1028B

Bebbington, M. S., & Marzocchi, W. (2011). Stochastic models for earthquake triggering of volcanic eruptions. *Journal of Geophysical Research*, *116*, B05204. https://doi.org/10.1029/2010JB008114

Berardino, P., Fornaro, G., Lanari, R., & Sansosti, E. (2002). A new algorithm for surface deformation monitoring based on small baseline differential SAR interferograms. *IEEE Transactions on Geoscience and Remote Sensing*, *40*(11), 2375–2383. https://doi.org/10.1109/TGRS.2002.803792

Bernard, A., & Mazot, A. (2004). Geochemical evolution of the young crater lake of Kelud volcano in Indonesia. *Water-Rock Interaction*, 87–90.

Biggs, J., Anthony, E. Y., & Ebinger, C. J. (2009). Multiple inflation and deflation events at Kenyan volcanoes, East African Rift. *Geology*, *37*(11), 979–982. https://doi.org/10.1130/G30133A.1

Biggs, J., Bastow, I. D., Keir, D., & Lewi, E. (2011). Pulses of deformation reveal frequently recurring shallow magmatic activity beneath the Main Ethiopian Rift. *Geochemistry, Geophysics, Geosystems*, *12*, Q0AB10. https://doi.org/10.1029/2011GC003662

Biggs, J., Ebmeier, S. K., Aspinall, W. P., Lu, Z., Pritchard, M. E., Sparks, R. S. J., & Mather, T. A. (2014). Global link between deformation and volcanic eruption quantified by satellite imagery. *Nature Communications*, *5*(1), 3471. https://doi.org/10.1038/ncomms4471

Biggs, J., & Pritchard, M. E. (2017). Global volcano monitoring: What does it mean when volcanoes deform? *Elements*, *13*(1), 17–22. https://doi.org/10.2113/gselements.13.1.17

Blake, S. (1984). Volatile oversaturation during the evolution of silicic magma chambers as an eruption trigger. *Journal of Geophysical Research*, *89*(B10), 8237–8244. https://doi.org/10.1029/JB089iB10p08237

Blundy, J., Cashman, K. V., Rust, A., & Witham, F. (2010). A case for CO_2-rich arc magmas. *Earth and Planetary Science Letters*, *290*(3–4), 289–301. https://doi.org/10.1016/j.epsl.2009.12.013

Botcharnikov, R. E., Holtz, F., Almeev, R. R., Sato, H., & Behrens, H. (2008). Storage conditions and evolution of andesitic magma prior to the 1991–95 eruption of Unzen volcano: Constraints from natural samples and phase equilibria experiments. *Journal of Volcanology and Geothermal Research*, *175*(1–2), 168–180. https://doi.org/10.1016/j.jvolgeores.2008.03.026

Bourdier, J.-L., Pratomo, I., Thouret, J.-C., & Vincent, P. M. (1997). Observations, stratigraphy and eruptive processes of the 1990 eruption of Kelut volcano, Indonesia. *Journal of Volcanology and Geothermal Research*, *79*(3–4), 181–203. https://doi.org/10.1016/S0377-0273(97)00031-0

Bouvet de Maisonneuve, C. (2015). Mafic magma replenishment, unrest, and eruption in a caldera setting: insights from the 2006 eruption of Rabaul (Papua New Guinea). *Chemical, Physical, and Temporal Evolution of Magmatic Systems*, *422*(1), 17–39. https://doi.org/http://doi.org/10.1144/SP422.2

Browne, B., Izbekov, P., Eichelberger, J., & Churikova, T. (2010). Preeruptive storage conditions of the Holocene dacite erupted from Kizimen Volcano, Kamchatka. *International Geology Review*, *52*(1), 95–110. https://doi.org/10.1080/00206810903332413

Cadoux, A., Scaillet, B., Druitt, T. H., & Deloule, E. (2014). Magma storage conditions of large plinian eruptions of santorini volcano (Greece). *Journal of Petrology*, *55*(6), 1129–1171. https://doi.org/10.1093/petrology/egu021

Caricchi, L., Annen, C., Blundy, J., Simpson, G., & Pinel, V. (2014). Frequency and magnitude of volcanic eruptions controlled by magma injection and buoyancy. *Nature Geoscience*, *7*(2), 126–130. https://doi.org/10.1038/ngeo2041

Caricchi, L., & Blundy, J. (2015). Experimental petrology of monotonous intermediate magmas. *Geological Society, London, Special Publications*, *422*(1), 105–130. https://doi.org/10.1144/SP422.9

Caricchi, L., Sheldrake, T. E., & Blundy, J. (2018). Modulation of magmatic processes by CO2 flushing. *Earth and Planetary Science Letters*, *491*, 160–171. https://doi.org/10.1016/J.EPSL.2018.03.042

Cassidy, M., Castro, J. M., Helo, C., Troll, V. R., Deegan, F. M., Muir, D., et al. (2016). Volatile dilution during magma injections and implications for volcano explosivity. *Geology*, *44*(12), 1027–1030. https://doi.org/10.1130/G38411.1

Cassidy, M., Manga, M., Cashman, K., & Bachmann, O. (2018). Controls on explosive-effusive volcanic eruption styles. *Nature Communications*, *9*(1), 2839. https://doi.org/10.1038/s41467-018-05293-3

Castro, J. M., & Dingwell, D. B. (2009). Rapid ascent of rhyolitic magma at Chaitén volcano, Chile. *Nature*, *461*(7265), 780–783. https://doi.org/10.1038/nature08458

Castro, J. M., Schipper, C. I., Mueller, S. P., Militzer, A. S., Amigo, A., Parejas, C. S., & Jacob, D. (2013). Storage and eruption of near-liquidus rhyolite magma at Cordón Caulle, Chile. *Bulletin of Volcanology*, *75*(4), 1–17. https://doi.org/10.1007/s00445-013-0702-9

Castruccio, A., Clavero, J., Segura, A., Samaniego, P., Roche, O., Le Pennec, J.-L., & Droguett, B. (2016). Eruptive parameters and dynamics of the April 2015 sub-Plinian eruptions of Calbuco volcano (southern Chile). *Bulletin of Volcanology*, *78*(9), 62. https://doi.org/10.1007/s00445-016-1058-8

Castruccio, A., Diez, M., & Gho, R. (2017). The Influence of Plumbing System Structure on Volcano Dimensions and Topography. *Journal of Geophysical Research: Solid Earth*, *122*, 8839–8859. https://doi.org/10.1002/2017JB014855

Caudron, C., Mazot, A., & Bernard, A. (2012). Carbon dioxide dynamics in Kelud volcanic lake. *Journal of Geophysical Research*, *117*, B05102. https://doi.org/10.1029/2011JB008806

Caudron, C., Taisne, B., Garcés, M., Alexis, L. P., & Mialle, P. (2015). On the use of remote infrasound and seismic stations to constrain the eruptive sequence and intensity for the 2014 Kelud eruption. *Geophysical Research Letters*, *42*, 6614–6621. https://doi.org/10.1002/2015GL064885

Chaussard, E., & Amelung, F. (2012). Precursory inflation of shallow magma reservoirs at west Sunda volcanoes detected by InSAR. *Geophysical Research Letters*, *39*, L21311. https://doi.org/10.1029/2012GL053817

Colbachini, R., Uantika, G., Jp, M., & Le Pichon, A., Pratomo, I., Murjaya, J. (2016). Monitoring of the February 2014 eruption of Kelud volcano using infraound and seismic small aperture arrays. In *Southeast Asian Conference on Geophysics 2016*.

Coombs, M. L., Eichelberger, J. C., & Rutherford, M. J. (2000). Magma storage and mixing conditions for the 1953-1974 eruptions of Southwest Trident volcano, Katmai National Park, Alaska. *Contributions to Mineralogy and Petrology*, *140*(1), 99–118. https://doi.org/10.1007/s004100000166

Coombs, M. L., & Gardner, J. E. (2002). Shallow-storage conditions for the rhyolite of the 1912 eruption at Novarupta, Alaska. *Geology*, *29*(9), 775–778. https://doi.org/10.1130/0091-7613(2001)029<0775:SSCFTR>2.0.CO;2

Cooper, K. M., & Kent, A. J. R. (2014). Rapid remobilization of magmatic crystals kept in cold storage. *Nature*, *506*(7489), 480–483. https://doi.org/10.1038/nature12991

Costa, F. (2004). Petrological and Experimental Constraints on the Pre-eruption Conditions of Holocene Dacite from Volcan San Pedro (36 S, Chilean Andes) and the Importance of Sulphur in Silicic Subduction-related Magmas. *Journal of Petrology*, *45*(4), 855–881. https://doi.org/10.1093/petrology/egg114

Costa, F., Andreastuti, S., Bouvet de Maisonneuve, C., & Pallister, J. S. (2013). Petrological insights into the storage conditions, and magmatic processes that yielded the centennial 2010 Merapi explosive eruption. *Journal of Volcanology and Geothermal Research*, *261*, 209–235. https://doi.org/10.1016/j.jvolgeores.2012.12.025

Couch, S., Sparks, R. S. J., & Carroll, M. R. (2003). The Kinetics of Degassing-Induced Crystallization at Soufrière Hills Volcano, Montserrat. *Journal of Petrology*, *44*(8), 1477–1502. https://doi.org/10.1093/petrology/44.8.1477

Davidson, J. P., Hora, J. M., Garrison, J. M., & Dungan, M. A. (2005). Crustal forensics in arc magmas. *Journal of Volcanology and Geothermal Research*, *140*(1–3), 157–170. https://doi.org/10.1016/j.jvolgeores.2004.07.019

Degruyter, W., Huber, C., Bachmann, O., Cooper, K. M., & Kent, A. J. R. (2017). Influence of Exsolved Volatiles on Reheating Silicic Magmas by Recharge and Consequences for Eruptive Style at Volcán Quizapu (Chile). *Geochemistry, Geophysics, Geosystems*, *18*, 4123–4135. https://doi.org/10.1002/2017GC007219

Delgado, F., Pritchard, M. E., Ebmeier, S., González, P., & Lara, L. (2017). Recent unrest (2002–2015) imaged by space geodesy at the highest risk Chilean volcanoes: Villarrica,Llaima, and Calbuco (Southern Andes). *Journal of Volcanology and GeothermalResearch*, *344*, 270–288. https://doi.org/10.1016/J.JVOLGEORES.2017.05.020 DeMets, C., Gordon, R. G., Argus, D. F., & Stein, S. (1990). Current plate motions. *Geophysical Journal International*, *101*(2), 425–478. https://doi.org/10.1111/j.1365-246X.1990.tb06579.x

de Novellis, V., Castaldo, R., de Luca, C., Pepe, S., Zinno, I., Casu, F., et al. (2017). Source modelling of the 2015 Wolf volcano (Galápagos) eruption inferred from Sentinel 1-A DInSAR deformation maps and preeruptive ENVISAT time series. *Journal of Volcanology and Geothermal Research*, *344*, 246–256. https://doi.org/10.1016/J.JVOLGEORES.2017.05.013

Druitt, T. H., Costa, F., Deloule, E., Dungan, M., & Scaillet, B. (2012). Decadal to monthly timescales of magma transfer and reservoir growth at a caldera volcano. *Nature*, *482*(7383), 77–80. https://doi.org/10.1038/nature10706

Druitt, T. H., Kokelaar, B. P., & Francis, P. (2004). The eruption of Soufrière Hills volcano, Montserrat, from 1995 to 1999. Geological Society, London, Memoirs (Vol. 29). https://doi.org/0435-4052/02/$15

Ebmeier, S. K., Andrews, B. J., Araya, M. C., Arnold, D. W. D., Biggs, J., Cooper, C., et al. (2018). Synthesis of global satellite observations of magmatic and volcanic deformation: implications for volcano monitoring & the lateral extent of magmatic domains. *Journal of Applied Volcanology*, *7*(1), 1–26. https://doi.org/10.1186/s13617-018-0071-3

Edmonds, M., Kohn, S. C., Hauri, E. H., Humphreys, M. C. S., & Cassidy, M. (2016). Extensive, water-rich magma reservoir beneath southern Montserrat. *Lithos*, *252-253*, 216–233. https://doi.org/10.1016/j.lithos.2016.02.026

Eichelberger, J. C., Carrigan, C. R., Westrich, H. R., & Price, R. H. (1986). Non-explosive silicic volcanism. *Nature*, *323*(6089), 598–602. https://doi.org/10.1038/323598a0

Elders, W. A., Friðleifsson, G. Ó., Zierenberg, R. A., Pope, E. C., Mortensen, A. K., Guðmundsson, Á., et al. (2011). Origin of a rhyolite that intruded a geothermal well while drilling at the Krafla volcano, Iceland. *Geology*, *39*(3), 231–234. https://doi.org/10.1130/G31393.1

Endo, E., Malone, S., Noson, L., & Weaver, C. (1981). *Locations, magnitudes, and statistics of the March 20-May 18 earthquake sequence. In The 1980 Eruptions of Mount St. Helens*, (pp. 93–108). Washington.

Erdmann, S., Martel, C., Pichavant, M., Bourdier, J. L., Champallier, R., Komorowski, J. C., & Cholik, N. (2016). Constraints from phase equilibrium experiments on preeruptive storage conditions in mixed magma systems: A case study on crystal-rich basaltic andesites from Mount Merapi, Indonesia. *Journal of Petrology*, *57*(3), 535–560. https://doi.org/10.1093/petrology/egw019

Ferretti, A., Fumagalli, A., Novali, F., Prati, C., Rocca, F., & Rucci, A. (2011). A New Algorithm for Processing Interferometric Data-Stacks: SqueeSAR. *IEEE Transactions on Geoscience and Remote Sensing*, *49*(9), 3460–3470. https://doi.org/10.1109/TGRS.2011.2124465

First, E., Hammer, J. E., & Ruprecht, P. (2017). Experimental constraints on dacite magma storage beneath Volcán Quizapu, Chile. In IAVCEI Scientific Assembly. Portland, Oregon.

Fowler, S. J., & Spera, F. J. (2008). Phase equilibria trigger for explosive volcanic eruptions. *Geophysical Research Letters*, *35*, L08309. https://doi.org/10.1029/2008GL033665

Freymueller, J. T., & Kaufman, A. M. (2010). Changes in the magma system during the 2008 eruption of Okmok volcano, Alaska, based on GPS measurements. *Journal of Geophysical Research*, *115*, B12415. https://doi.org/10.1029/2010JB007716

Furtney, M. A., Pritchard, M. E., Ebmeier, S. K., Jay, J. A., Carn, S. A., McCormick, B. T., & Reath, K. (2018). Synthesizing multi-sensor, multi-satellite, multi-decadal data sets for global volcano monitoring. *Journal of Volcanology and Geothermal Research*, *365*, 38–56. https://doi.org/10.1016/j.jvolgeores.2018.10.002

Gardner, C. A., Cashman, K. V., & Neal, C. A. (1998). Tephra-fall deposits from the 1992 eruption of Crater Peak, Alaska: implications of clast textures for eruptive processes. *Bulletin of Volcanology*, *59*(8), 537–555. https://doi.org/10.1007/s004450050208

Girona, T., Costa, F., & Schubert, G. (2016). Degassing during quiescence as a trigger of magma ascent and volcanic eruptions. *Scientific Reports*, *5*(1), 18212. https://doi.org/10.1038/srep18212

Global Volcanism Program, Smithsonian Institution. (2013). Retrieved from https://volcano.si.edu/gvp_termsofuse.cfm

Goitom, B., Oppenheimer, C., Hammond, J. O. S., Grandin, R., Barnie, T., Donovan, A., et al. (2015). First recorded eruption of Nabro volcano, Eritrea, 2011. *Bulletin of Volcanology*, *77*(10), 85. https://doi.org/10.1007/s00445-015-0966-3

Gonnermann, H. M., & Manga, M. (2003). Explosive volcanism may not be an inevitable consequence of magma fragmentation. *Nature*, *426*(6965), 432–435. https://doi.org/10.1038/nature02138

Gonnermann, H. M., & Manga, M. (2007). The fluid mechanics inside a volcano. *Annual Review of Fluid Mechanics*, *39*(1), 321–356. https://doi.org/10.1146/annurev.fluid.39.050905.110207

Goode, L. R., Handley, H. K., Cronin, S. J., & Abdurrachman, M. (2018). Insights into eruption dynamics from the 2014 pyroclastic deposits of Kelut volcano, Java, Indonesia, and implications for future hazards. *Journal of Volcanology and Geothermal Research*. https://doi.org/10.1016/j.jvolgeores.2018.02.005

Grove, T. L., Elkins-Tanton, L. T., Parman, S. W., Chatterjee, N., Müntener, O., & Gaetani, G. A. (2003). Fractional crystallization and mantle-melting controls on calc-alkaline differentiation trends. *Contributions to Mineralogy and Petrology*, *145*(5), 515–533. https://doi.org/10.1007/s00410-003-0448-z

Hall, M., Ramón, P., Mothes, P., LePennec, J. L., García, A., Samaniego, P., & Yepes, H. (2004). Volcanic eruptions with little warning: the case of Volcán Reventador's Surprise November 3, 2002 Eruption, Ecuador. *Revista Geológica de Chile*, *31*(2), 349–358. https://doi.org/10.4067/S0716-02082004000200010

Hamada, M., Okayama, Y., Kaneko, T., Yasuda, A., & Fujii, T. (2014). Polybaric crystallization differentiation of H2O-saturated island arc low-K tholeiite magmas: A case study of the Izu-Oshima volcano in the Izu arc. *Earth, Planets and Space*, *66*(1), 15. https://doi.org/10.1186/1880-5981-66-15

Hamiel, Y., & Baer, G. (2016). Crustal deformation associated with the 2011 eruption of the Nabro volcano, Eritrea. *Tectonophysics*, *691*, 257–262. https://doi.org/10.1016/J.TECTO.2016.10.013

Hamlyn, J., Wright, T., Walters, R., Pagli, C., Sansosti, E., Casu, F., et al. (2018). What causes subsidence following the 2011 eruption at Nabro (Eritrea)? *Progress in Earth and Planetary Science*, *5*(1), 31. https://doi.org/10.1186/s40645-018-0186-5

Hamlyn, J. E., Keir, D., Wright, T. J., Neuberg, J. W., Goitom, B., Hammond, J. O. S., et al. (2014). Seismicity and subsidence following the 2011 Nabro eruption, Eritrea: Insights into the plumbing system of an off-rift volcano. *Journal of Geophysical Research: Solid Earth*, *119*, 8267–8282. https://doi.org/10.1002/2014JB011395

Hammer, J. E., Rutherford, M. J., & Hildreth, W. (2002). Magma storage prior to the 1912 eruption at Novarupta, Alaska. *Contributions to Mineralogy and Petrology*, *144*(2), 144–162. https://doi.org/10.1007/s00410-002-0393-2

Hidayati, S., Basuki, A., Kristianto, K., & Mulyana, I. (2011). Emergence of lava dome from the crater lake of Kelud Volcano, East Java. Indones. *Journal of Geosciences*, *4*(4), 229–238.

Hidayati, S., Triastuty, H., Mulyana, I., Adi, S., Ishihara, K., Basuki, A., et al. (2018). Differences in the seismicity preceding the 2007 and 2014 eruptions of Kelud volcano, Indonesia. *Journal of Volcanology and Geothermal Research*. https://doi.org/10.1016/j.jvolgeores.2018.10.017

Holtz, F., Sato, H., Lewis, J., Behrens, H., & Nakada, S. (2005). Experimental petrology of the 1991-1995 Unzen dacite, Japan. Part I: Phase relations, phase composition and preeruptive conditions. *Journal of Petrology*, *46*(2), 319–337. https://doi.org/10.1093/petrology/egh077

Hooper, A., Zebker, H., Segall, P., & Kampes, B. (2004). A new method for measuring deformation on volcanoes and other natural terrains using InSAR persistent scatterers. *Geophysical Research Letters*, *31*, L23611. https://doi.org/10.1029/2004GL021737

Hreinsdóttir, S., Sigmundsson, F., Roberts, M. J., Björnsson, H., Grapenthin, R., Arason, P., et al. (2014). Volcanic plume height correlated with magma-pressure change at Grímsvötn Volcano, Iceland. *Nature Geoscience*, *7*(3), 214–218. https://doi.org/10.1038/ngeo2044

Ishihara, K., Hendrasto, M., & Hidayati, S. (2011). Long-term forecasting of volcanic eruption in case of Kelud volcano, Indonesia. *Annuals Disaster Prevention Research Institute, Kyoto University*, *54*, 209–214.

Jaupart, C., & Allègre, C. J. (1991). Gas content, eruption rate and instabilities of eruption regime in silicic volcanoes. *Earth and Planetary Science Letters*, *102*(3–4), 413–429. https://doi.org/10.1016/0012-821X(91)90032-D

Jay, J., Costa, F., Pritchard, M., Lara, L., Singer, B., & Herrin, J. (2014). Locating magma reservoirs using InSAR and petrology before and during the 2011–2012 Cordón Caulle silicic eruption. *Earth and Planetary Science Letters*, *395*, 254–266. https://doi.org/10.1016/j.epsl.2014.03.046

Jeffery, A. J., Gertisser, R., Troll, V. R., Jolis, E. M., Dahren, B., Harris, C., et al. (2013). The preeruptive magma plumbing system of the 2007–2008 dome-forming eruption of Kelut volcano, East Java, Indonesia. *Contributions to Mineralogy and Petrology*, *166*(1), 275–308. https://doi.org/10.1007/s00410-013-0875-4

Kilbride, B. M., Edmonds, M., & Biggs, J. (2016). Observing eruptions of gas-rich compressible magmas from space. *Nature Communications*, *7*(1), 13744. https://doi.org/10.1038/ncomms13744

Koleszar, A. M., Kent, A. J. R., Wallace, P. J., & Scott, W. E. (2012). Controls on long-term low explosivity at andesitic arc volcanoes: Insights from Mount Hood, Oregon. *Journal of Volcanology and Geothermal Research*, *219-220*, 1–14. https://doi.org/10.1016/j.jvolgeores.2012.01.003

Kopp, H., Flueh, E. R., Petersen, C. J., Weinrebe, W., Wittwer, A., & Scientists, M. (2006). The Java margin revisited: Evidence for subduction erosion off Java. *Earth and Planetary Science Letters*, *242*(1–2), 130–142. https://doi.org/10.1016/J.EPSL.2005.11.036

Krischer, L., Megies, T., Barsch, R., Beyreuther, M., Lecocq, T., Caudron, C., & Wassermann, J. (2015). ObsPy: a bridge for seismology into the scientific Python ecosystem. *Computational Science & Discovery*, *8*(1), 014003. https://doi.org/10.1088/1749-4699/8/1/014003

Kristiansen, N. I., Prata, A. J., Stohl, A., & Carn, S. A. (2015). Stratospheric volcanic ash emissions from the 13 February 2014 Kelut eruption. *Geophysical Research Letters*, *42*, 588–596. https://doi.org/10.1002/2014GL062307

Kusumadinata, K. (1979). Catalogue of references on Indonesian volcanoes with eruiptions in historical time. The Directorate of Volcanology Indonesia. Retrieved from https://ci.nii.ac.jp/naid/10005341070/

Larsen, J. F. (2006). Rhyodacite magma storage conditions prior to the 3430 yBP caldera-forming eruption of Aniakchak volcano, Alaska. *Contributions to Mineralogy and Petrology*, *152*(4), 523–540. https://doi.org/10.1007/s00410-006-0121-4

Lesage, P., Carrara, A., Pinel, V., & Arámbula-Mendoza, R. (2018). Absence of detectable precursory deformation and velocity variation before the large dome collapse of July 2015 at Volcán de Colima, Mexico. *Frontiers in Earth Science*, *6*, 93. https://doi.org/10.3389/feart.2018.00093

Lister, J. R., & Kerr, R. C. (1991). Fluid-mechanical models of crack propagation and their application to magma transport in dykes. *Journal of Geophysical Research*, *96*(B6), 10049. https://doi.org/10.1029/91JB00600

Loughlin, S., Sparks, S., Brown, S., Jenkins, S., & Vye-Brown, C. (Eds.). (2015). *Global volcanic hazards and risk*. Cambridge: Cambridge University Press. https://doi.org/0.1017/CBO9781316276273

Lu, Z., & Dzurisin, D. (2014). InSAR imaging of Aleutian volcanoes. In *InSAR imaging of Aleutian volcanoes*, (pp. 87–345). Berlin, Heidelberg: Springer Berlin Heidelberg. https://doi.org/10.1007/978-3-642-00348-6_6

Lu, Z., Dzurisin, D., Biggs, J., Wicks, C., & McNutt, S. (2010). Ground surface deformation patterns, magma supply, and magma storage at Okmok volcano, Alaska, from InSAR analysis: 1. Intereruption deformation, 1997–2008. *Journal of Geophysical Research*, *115*, B00B02. https://doi.org/10.1029/2009JB006969

Luhr, J. F. (1990). Experimental phase-relations of water-saturated and sulfur-saturated arc magmas and the 1982 eruptions of El-Chichon volcano. *Journal of Petrology*, *31*(5), 1071–1114. https://doi.org/10.1093/petrology/31.5.1071

Lundgren, P., Kiryukhin, A., Milillo, P., & Samsonov, S. (2015). Dike model for the 2012–2013 Tolbachik eruption constrained by satellite radar interferometry observations. *Journal of Volcanology and Geothermal Research*, *307*, 79–88. https://doi.org/10.1016/J.JVOLGEORES.2015.05.011

Maeno, F., Nakada, S., Yoshimoto, M., Shimano, T., Hokanishi, N., Zaennudin, A., & Iguchi, M. (2016). A sequence of a plinian eruption preceded by dome destruction at Kelud volcano, Indonesia, on February 13, 2014, revealed from tephra fallout and pyroclastic density current deposits. *Journal of Volcanology and Geothermal Research*. https://doi.org/10.1016/j.jvolgeores.2017.03.002

Magee, C., Stevenson, C. T. E., Ebmeier, S. K., Keir, D., Hammond, J. O. S., Gottsmann, J. H., et al. (2018). Magma plumbing systems: A geophysical perspective. *Journal of Petrology*, *59*(6), 1217–1251. https://doi.org/10.1093/petrology/egy064

Martel, C., Pichavant, M., Bourdier, J. L., Traineau, H., Holtz, F., & Scaillet, B. (1998). Magma storage conditions and control of eruption regime in silicic volcanoes: experimental evidence from Mt. *Pelée. Earth and Planetary Science Letters*, *156*(1–2), 89–99. https://doi.org/10.1016/S0012-821X(98)00003-X

Martin, V. M., Morgan, D. J., Jerram, D. A., Caddick, M. J., Prior, D. J., & Davidson, J. P. (2008). Bang! Month-scale eruption triggering at santorini volcano. *Science*, *321*(5893), 1178. https://doi.org/10.1126/science.1159584

Marzocchi, W., & Bebbington, M. S. (2012). Probabilistic eruption forecasting at short and long time scales. *Bulletin of Volcanology*, *74*(8), 1777–1805. https://doi.org/10.1007/s00445-012-0633-x

Matoza, R. S., Fee, D., Green, D. N., le Pichon, A., Vergoz, J., Haney, M. M., et al. (2018). Local, regional, and remote seismo-acoustic observations of the April 2015 VEI 4 eruption of Calbuco volcano, Chile. *Journal of Geophysical Research: Solid Earth*, *123*, 3814–3827. https://doi.org/10.1002/2017JB015182

Matoza, R. S., Landès, M., Le Pichon, A., Ceranna, L., & Brown, D. (2013). Coherent ambient infrasound recorded by the International Monitoring System. *Geophysical Research Letters*, *40*, 429–433. https://doi.org/10.1029/2012GL054329

McCanta, M. C., Rutherford, M. J., & Hammer, J. E. (2007). Preeruptive and syn-eruptive conditions in the Black Butte, California dacite: Insight into crystallization kinetics in a silicic magma system. *Journal of Volcanology and Geothermal Research*, *160*(3–4), 263–284. https://doi.org/10.1016/j.jvolgeores.2006.10.004

Miwa, T., Toramaru, A., & Iguchi, M. (2009). Correlations of volcanic ash texture with explosion earthquakes from vulcanian eruptions at Sakurajima volcano, Japan. *Journal of Volcanology and Geothermal Research*, *184*(3–4), 473–486. https://doi.org/10.1016/j.jvolgeores.2009.05.012

Mogi, K. (1958). Relations between the eruptions of various volcanoes and the deformations of the ground surfaces around them. *Bulletin of the Earthquake Research Institute*, *36*, 99–134.

Moore, G. (2008). Interpreting H_2O and CO_2 contents in melt inclusions: Constraints from solubility experiments and modeling. *Reviews in Mineralogy and Geochemistry*, *69*(1), 333–362. https://doi.org/10.2138/rmg.2008.69.9

Moore, G., & Carmichael, I. S. E. (1998). The hydrous phase equilibira (to 3 kbar) of an andesite and basaltic andesite from western Mexico: Constraints on water content and conditions of phenocryst growth. *Contributions to Mineralogy and Petrology*, *130*(3-4), 304–319. https://doi.org/10.1007/s004100050367

Muir, D., Blundy, D., Rust, A. C., & Hickey, J. (2014). Experimental constraints on dacite preeruptive magma storage conditions beneath Uturuncu volcano. *Journal of Petrology*, *55*(4), 749–767. https://doi.org/10.1093/petrology/egu005

Muir, D. D., Blundy, J. D., & Rust, A. C. (2012). Multiphase petrography of volcanic rocks using element maps: A method applied to Mount St. Helens, 1980–2005. *Bulletin of Volcanology*, *74*(5), 1101–1120. https://doi.org/10.1007/s00445-012-0586-0

Myers, M. L., Wallace, P. J., Wilson, C. J. N., Morter, B. K., & Swallow, E. J. (2016). Prolonged ascent and episodic venting of discrete magma batches at the onset of the Huckleberry Ridge supereruption, Yellowstone. *Earth and Planetary Science Letters*, *451*, 285–297. https://doi.org/10.1016/j.epsl.2016.07.023

Nakamichi, H., Iguchi, M., Triastuty, H., Hendrasto, M., & Mulyana, I. (2017). Differences of precursory seismic energy release for the 2007 effusive dome-forming and 2014 Plinian eruptions at Kelud volcano, Indonesia. *Journal of Volcanology and Geothermal Research*. https://doi.org/10.1016/j.jvolgeores.2017.08.004

Nakashima, Y., Heki, K., Takeo, A., Cahyadi, M. N., Aditiya, A., & Yoshizawa, K. (2016). Atmospheric resonant oscillations by the 2014 eruption of the Kelud volcano, Indonesia, observed with the ionospheric total electron contents and seismic signals. *Earth and Planetary Science Letters*, *434*, 112–116. https://doi.org/10.1016/j.epsl.2015.11.029

Owen, J., Tuffen, H., & McGarvie, D. W. (2013). Explosive subglacial rhyolitic eruptions in Iceland are fuelled by high magmatic H_2O and closed-system degassing. *Geology*, *41*(2), 251–254. https://doi.org/10.1130/G33647.1

Pallister, J., & McNutt, S. R. (2015). *Synthesis of volcano monitoring. The encyclopedia of volcanoes*, (p. 1456). Elsevier Inc. https://doi.org/10.1016/B978-0-12-385938-9.00066-3

Pallister, J. S., Hoblitt, R. P., & Reyes, A. G. (1992). A basalt trigger for the 1991 eruptions of Pinatubo volcano? *Nature*, *356*(6368), 426–428. https://doi.org/10.1038/356426a0

Pallister, J. S., Schneider, D. J., Griswold, J. P., Keeler, R. H., Burton, W. C., Noyles, C., et al. (2013). Merapi 2010 eruption—Chronology and extrusion rates monitored with satellite radar and used in eruption forecasting. *Journal of Volcanology and Geothermal Research*, *261*, 144–152. https://doi.org/10.1016/j.jvolgeores.2012.07.012

Papale, P., Moretti, R., & Barbato, D. (2006). The compositional dependence of the saturation surface of $H_2O + CO_2$ fluids in silicate melts. *Chemical Geology*, *229*(1–3), 78–95. https://doi.org/10.1016/j.chemgeo.2006.01.013

Parat, F., Streck, M. J., Holtz, F., & Almeev, R. (2014). Experimental study into the petrogenesis of crystal-rich basaltic to andesitic magmas at Arenal volcano. *Contributions to Mineralogy and Petrology*, *168*(2), 1–18. https://doi.org/10.1007/s00410-014-1040-4

Parat, F., Holtz, F., & Feig, S. (2008). Preeruptive conditions of the Huerto Andesite (Fish canyon system, San Juan volcanic field, Colorado): Influence of volatiles (C-O-H-S) on phase equilibria and mineral composition. *Journal of Petrology*, *49*(5), 911–935. https://doi.org/10.1093/petrology/egn011

Parks, M. M., Biggs, J., England, P., Mather, T. A., Nomikou, P., Palamartchouk, K., et al. (2012). Evolution of Santorini Volcano dominated by episodic and rapid fluxes of melt from depth. *Nature Geoscience*, *5*(10), 749–754. https://doi.org/10.1038/ngeo1562

Passarelli, L., & Brodsky, E. E. (2012). The correlation between run-up and repose times of volcanic eruptions. *Geophysical Journal International*, *188*(3), 1025–1045. https://doi.org/10.1111/j.1365-246X.2011.05298.x

Pertermann, M., & Lundstrom, C. C. (2006). Phase equilibrium experiments at 0.5 GPa and 1100–1300 °C on a basaltic andesite from Arenal volcano, Costa Rica. *Journal of Volcanology and Geothermal Research*, *157*(1–3), 222–235. https://doi.org/10.1016/j.jvolgeores.2006.03.043

Petrelli, M., El Omari, K., Spina, L., Le Guer, Y., La Spina, G., & Perugini, D. (2018). Timescales of water accumulation in magmas and implications for short warning times of explosive eruptions. *Nature Communications*, *9*(1). https://doi.org/10.1038/s41467-018-02987-6

Philibosian, B., & Simons, M. (2011). A survey of volcanic deformation on Java using ALOS PALSAR interferometric time series. *Geochemistry, Geophysics, Geosystems*, *12*, Q11004. https://doi.org/10.1029/2011GC003775

Phillipson, G., Sobradelo, R., & Gottsmann, J. (2013). Global volcanic unrest in the 21st century: An analysis of the first decade. *Journal of Volcanology and Geothermal Research*, *264*, 183–196. https://doi.org/10.1016/j.jvolgeores.2013.08.004

Pichavant, M., Costa, F., Burgisser, A., Scaillet, B., Martel, C., & Poussineau, S. (2007). Equilibration scales in silicic to intermediate magmas—Implications for experimental studies. *Journal of Petrology*, *48*(10), 1955–1972. https://doi.org/10.1093/petrology/egm045

Pichavant, M., Martel, C., Bourdier, J.-L., & Scaillet, B. (2002). Physical conditions, structure, and dynamics of a zoned magma chamber: Mount Pelée (Martinique, Lesser Antilles Arc). *Journal of Geophysical Research*, *107*(B5), 2093. https://doi.org/10.1029/2001jb000315

Pinel, V., & Jaupart, C. (2000). The effect of edifice load on magma ascent beneath a volcano. *Philosophical Transactions of the Royal Society A: Mathematical, Physical and Engineering Sciences*, *358*(1770), 1515–1532. https://doi.org/10.1098/rsta.2000.0601

Pinel, V., & Jaupart, C. (2004). Magma storage and horizontal dyke injection beneath a volcanic edifice. *Earth and Planetary Science Letters*, *221*(1–4), 245–262. https://doi.org/10.1016/S0012-821X(04)00076-7

Pinel, V., Poland, M. P., & Hooper, A. (2014). Volcanology: Lessons learned from Synthetic Aperture Radar imagery. *Journal of Volcanology and Geothermal Research*, *289*, 81–113. https://doi.org/10.1016/j.jvolgeores.2014.10.010

Plank, T., & Langmuir, C. H. (1998). The chemical composition of subducting sediment and its consequences for the crust and mantle. *Chemical Geology.*, *145*(3-4), 325–394. https://doi.org/10.1016/S0009-2541(97)00150-2

Power, J., Jolly, A., & C., N., & M., H. (2002). A conceptual model of the Mount Spurr magmatic system from seismic and geochemical observations of the 1992 Crater Peak eruption sequence. *Bulletin of Volcanology*, *64*(3–4), 206–218. https://doi.org/10.1007/s00445-002-0201-x

Preece, K., Barclay, J., Gertisser, R., & Herd, R. A. (2013). Textural and micro-petrological variations in the eruptive products of the 2006 dome-forming eruption of Merapi volcano, Indonesia: Implications for sub-surface processes. *Journal of Volcanology and Geothermal Research*, *261*, 98–120. https://doi.org/10.1016/j.jvolgeores.2013.02.006

Pritchard, M. E., Mather, T. A., McNutt, S. R., Delgado, F. J., & Reath, K. (2019). Thoughts on the criteria to determine the origin of volcanic unrest as magmatic or non-magmatic. *Philosophical Transactions of the Royal Society A: Mathematical, Physical and Engineering Sciences*, *377*(2139). https://doi.org/10.1098/rsta.2018.0008

Pyle, D. M. (2017). What can we learn from records of past eruptions to better prepare for the future? *Advances in Volcanology*. https://doi.org/10.1007/11157_2017_5

Rasmussen, D. J., Plank, T. A., Roman, D. C., Power, J. A., Bodnar, R. J., & Hauri, E. H. (2018). When does eruption run-up begin? Multidisciplinary insight from the 1999 eruption of Shishaldin volcano. *Earth and Planetary Science Letters*, *486*, 1–14. https://doi.org/10.1016/J.EPSL.2018.01.001

Reverso, T., Vandemeulebrouck, J., Jouanne, F., Pinel, V., Villemin, T., Sturkell, E., & Bascou, P. (2014). A two-magma chamber model as a source of deformation at Grímsvötn Volcano, Iceland. *Journal of Geophysical Research: Solid Earth*, *119*, 4666–4683. https://doi.org/10.1002/2013JB010569

Rubin, A. E., Cooper, K. M., Till, C. B., Kent, A. J. R., Costa, F., Bose, M., et al. (2017). Rapid cooling and cold storage in a silicic magma reservoir recorded in individual crystals. *Science*, *356*(6343), 1154–1156. https://doi.org/10.1126/SCIENCE.AAM8720

Ruppert, N. A., Prejean, S., & Hansen, R. A. (2011). Seismic swarm associated with the 2008 eruption of Kasatochi Volcano, Alaska: Earthquake locations and source parameters. *Journal of Geophysical Research*, *116*, B00B07. https://doi.org/10.1029/2010JB007435

Ruprecht, P., & Bachmann, O. (2010). Preeruptive reheating during magma mixing at Quizapu volcano and the implications for the explosiveness of silicic arc volcanoes. *Geology*, *38*(10), 919–922. https://doi.org/10.1130/G31110.1

Rutherford, M. J., & Devine, J. D. (1988). The May 18, 1980, eruption of Mount St. Helens: 3. Stability and chemistry of amphibole in the magma chamber. *Journal of Geophysical Research*, *93*(B10), 11,949. https://doi.org/10.1029/JB093iB10p11949

Rutherford, M. J., & Devinel, J. D. (1996). Preeruption Pressure-Temperature Conditions and Volatiles in the I99l Dacitic Magma of Mount Pinatubo. In Fire and mud, eruptions and lahars of mount pinatubo, phillipines. Retrieved from https://pubs.usgs.gov/pinatubo/ruth/

Saepuloh, A., Koike, K., Omura, M., Iguchi, M., & Setiawan, A. (2010). SAR- and gravity change-based characterization of the distribution pattern of pyroclastic flow deposits at Mt. Merapi during the past 10 years. *Bulletin of Volcanology*, *72*(2), 221–232. https://doi.org/10.1007/s00445-009-0310-x

Scaillet, B., Pichavant, M., & Cioni, R. (2008). Upward migration of Vesuvius magma chamber over the past 20,000 years. *Nature*, *455*(7210), 216–219. https://doi.org/10.1038/nature07232

Scaillet, B., & Evans, B. W. (1999). The 15 June 1991 eruption of Mount Pinatubo. I. Phase equilibria and pre-eruption P-T-fO_2-fH_2O conditions of the dacite magma. *Journal of Petrology*, *40*(3), 381–411. https://doi.org/10.1093/petroj/40.3.381

Scandone, R., Cashman, K. V., & Malone, S. D. (2007). Magma supply, magma ascent and the style of volcanic eruptions. *Earth and Planetary Science Letters*, *253*(3–4), 513–529. https://doi.org/10.1016/j.epsl.2006.11.016

Scarlato, P., Mollo, S., del Bello, E., von Quadt, A., Brown, R. J., Gutierrez, E., et al. (2017). The 2013 eruption of Chaparrastique volcano (El Salvador): Effects of magma storage, mixing, and decompression. *Chemical Geology*, *448*, 110–122. https://doi.org/10.1016/j.chemgeo.2016.11.015

Schmidt, D. A., & Bürgmann, R. (2003). Time-dependent land uplift and subsidence in the Santa Clara valley, California, from a large interferometric synthetic aperture radar data set. *Journal of Geophysical Research*, *108*(B9), 2416. https://doi.org/10.1029/2002JB002267

Scott, J. A. J., Mather, T. A., Pyle, D. M., Rose, W. I., & Chigna, G. (2012). The magmatic plumbing system beneath Santiaguito Volcano, Guatemala. *Journal of Volcanology and Geothermal Research*, *237-238*, 54–68. https://doi.org/10.1016/j.jvolgeores.2012.05.014

Shcherbakov, V. D., Neill, O. K., Izbekov, P. E., & Plechov, P. Y. (2013). Phase equilibria constraints on preeruptive magma storage conditions for the 1956 eruption of Bezymianny Volcano, Kamchatka, Russia. *Journal of Volcanology and Geothermal Research*, *263*, 132–140. https://doi.org/10.1016/j.jvolgeores.2013.02.010

Shea, T. (2017). Bubble nucleation in magmas: A dominantly heterogeneous process? *Journal of Volcanology and Geothermal Research*, *343*, 155–170. https://doi.org/10.1016/j.jvolgeores.2017.06.025

Shea, T., & Hammer, J. E. (2013). Oxidation in CSPV experiments involving H2O-bearing mafic magmas: Quantification and mitigation. *American Mineralogist*, *98*(7), 1285–1296. https://doi.org/10.2138/am.2013.4253

Shea, T., Houghton, B. F., Gurioli, L., Cashman, K. V., Hammer, J. E., & Hobden, B. J. (2010). Textural studies of vesicles in volcanic rocks: An integrated methodology. *Journal of Volcanology and Geothermal Research*, *190*(3–4), 271–289. https://doi.org/10.1016/j.jvolgeores.2009.12.003

Sigmundsson, F., Hreinsdóttir, S., Hooper, A., Árnadóttir, T., Pedersen, R., Roberts, M. J., et al. (2010). Intrusion triggering of the 2010 Eyjafjallajökull explosive eruption. *Nature*, *468*(7322), 426–430. https://doi.org/10.1038/nature09558

Simons, M., & Rosen, P. A. (2015). Interferometric synthetic aperture radar geodesy. In *Treatise on Geophysics* (Vol. 3, 2nd ed., pp. 339–385). https://doi.org/10.1016/B978-0-444-53802-4.00061-0Volume 3, Pages 339-385

Smith, V. C., Shane, P., & Nairn, I. A. (2005). Trends in rhyolite geochemistry, mineralogy, and magma storage during the last 50 kyr at Okataina and Taupo volcanic centres, Taupo Volcanic Zone, New Zealand. *Journal of Volcanology and Geothermal Research*, *148*(3–4), 372–406. https://doi.org/10.1016/J.JVOLGEORES.2005.05.005

Smyth, H. R., Hamilton, P. J., Hall, R., & Kinny, P. D. (2007). The deep crust beneath island arcs: Inherited zircons reveal a Gondwana continental fragment beneath East Java, Indonesia. *Earth and Planetary Science Letters*, *258*(1-2), 269–282. https://doi.org/10.1016/j.epsl.2007.03.044

Spaans, K., & Hooper, A. (2016). InSAR processing for volcano monitoring and other near-real time applications. *Journal of Geophysical Research: Solid Earth*, *121*, 2947–2960. https://doi.org/10.1002/2015JB012752

Sparks, R. S. J. (1997). Causes and consequences of pressurisation in lava dome eruptions. *Earth and Planetary Science Letters*, *150*(3–4), 177–189. https://doi.org/10.1016/S0012-821X(97)00109-X

Sparks, R. S. J. (2003). Forecasting volcanic eruptions. *Earth and Planetary Science Letters*, *210*(1–2), 1–15. https://doi.org/10.1016/S0012-821X(03)00124-9

Sparks, R. S. J., Biggs, J., & Neuberg, J. W. (2012). Monitoring volcanoes. *Science*, *335*(6074), 1310–1311. https://doi.org/10.1126/science.1219485

Stix, J. (2018). Understanding fast and slow unrest at volcanoes and implications for eruption forecasting. *Frontiers in Earth Science*, *6*(June). https://doi.org/10.3389/feart.2018.00056

Stock, M. J., Humphreys, M. C. S., Smith, V. C., Isaia, R., & Pyle, D. M. (2016). Late-stage volatile saturation as a potential trigger for explosive volcanic eruptions. *Nature Geoscience*, *9*(3), 249–254. https://doi.org/10.1038/ngeo2639

Surono, Jousset, P., Pallister, J., Boichu, M., Buongiorno, M. F., Budisantoso, A., et al. (2012). The 2010 explosive eruption of Java's Merapi volcano-A "100-year" event. *Journal of Volcanology and Geothermal Research*, *241-242*, 121–135. https://doi.org/10.1016/j.jvolgeores.2012.06.018

Surono, L. (1995). Seismic precursors of the February 10, 1990 eruption of Kelut volcano, Java. *Journal of Volcanology and Geothermal Research*, *65*(1–2), 135–146. https://doi.org/10.1016/0377-0273(94)00051-H

Suzuki, Y. J., & Iguchi, M. (2017). Determination of the mass eruption rate for the 2014 Mount Kelud eruption using three-dimensional numerical simulations of volcanic plumes. *Journal of Volcanology and Geothermal Research*. https://doi.org/10.1016/j.jvolgeores.2017.06.011

Tait, S., Jaupart, C., & Vergniolle, S. (1989). Pressure, gas content and eruption periodicity of a shallow, crystallising magma chamber. *Earth and Planetary Science Letters*, *92*(1), 107–123. https://doi.org/10.1016/0012-821X(89)90025-3

Tarasewicz, J., White, R. S., Woods, A. W., Brandsdóttir, B., & Gudmundsson, M. T. (2012). Magma mobilization by downward-propagating decompression of the Eyjafjallajkull volcanic plumbing system. *Geophysical Research Letters*, *39*, L19309. https://doi.org/10.1029/2012GL053518

Ten Brink, U. S., & Brocher, T. M. (1987). Multichannel seismic evidence for a subcrustal intrusive complex under Oahu and a model for Hawaiian volcanism. *Journal of Geophysical Research*, *92*(B13), 13,687–13,707. https://doi.org/10.1029/JB092iB13p13687

Thouret, J. C., Abdurachman, K. E., Bourdier, J. L., & Bronto, S. (1998). Origin, characteristics, and behaviour of lahars following the 1990 eruption of Kelud volcano, eastern Java (Indonesia). *Bulletin of Volcanology*, *59*(7), 460–480. https://doi.org/10.1007/s004450050204

Till, C. B., Vazquez, J. A., & Boyce, J. W. (2015). Months between rejuvenation and volcanic eruption at Yellowstone caldera, Wyoming. *Geology*, *43*(8), 695–698. https://doi.org/10.1130/G36862.1

Tilling, R. I. (2008). The critical role of volcano monitoring in risk reduction. *Advances in Geosciences*, *14*, 3–11. https://doi.org/10.5194/adgeo-14-3-2008

Toramaru, A. (2006). BND (bubble number density) decompression rate meter for explosive volcanic eruptions. *Journal of Volcanology and Geothermal Research*, *154*(3–4), 303–316. https://doi.org/10.1016/j.jvolgeores.2006.03.027

Tramontano, S., Gualda, G. A. R., & Ghiorso, M. S. (2017). Internal triggering of volcanic eruptions: tracking overpressure regimes for giant magma bodies. *Earth and Planetary Science Letters*, *472*, 142–151. https://doi.org/10.1016/j.epsl.2017.05.014

Tregoning, P., Brunner, F. K., Bock, Y., Puntodewo, S. S. O., McCaffrey, R., Genrich, J. F., et al. (1994). First geodetic measurement of convergence across the Java Trench. *Geophysical Research Letters*, *21*(19), 2135–2138. https://doi.org/10.1029/94GL01856

Triastuty, M. H., Hendrasto, G., Sunatika, I., Mulyana, S., Adi, K., Huda, B., et al. (2014). Chronology of 13 February 2014 Kelud eruption, Republic of Indonesia. Ministry of Energy and Mineral Resources, Republic of Indonesia.

Vandemeulebrouck, J., Sabroux, J. C., Halbwachs, M., Surono, P. N., Grangeon, J., & Tabbagh, J. (2000). Hydroacoustic noise precursors of the 1990 eruption of Kelut Volcano, Indonesia. *Journal of Volcanology and Geothermal Research*, *97*(1–4), 443–456. https://doi.org/10.1016/S0377-0273(99)00176-6

Venezky, D. Y., & Rutherford, M. J. (1997). Preeruption conditions and timing of dacite-andesite magma mixing in the 2.2 ka eruption at Mount Rainier. *Journal of Geophysical Research*, *102*(B9), 20,069–20,086. https://doi.org/10.1029/97jb01590

Venzke, E. (2013). Global Volcanism Program|Volcanoes of the World (VOTW) database information. Retrieved March 7, 2018, from http://volcano.si.edu/gvp_votw.cfm

Venzke, E. (2018). Global Volcanism Program|Volcanoes of the World (VOTW) database information. https://doi.org/https://doi.org/10.5479/si. GVP.VOTW4-2013

Wallace, P. J., Anderson, A. T., & Davis, A. M. (1999). Gradients in H_2O, CO_2, and exsolved gas in a large-volume silicic magma system: Interpreting the record preserved in melt inclusions from the Bishop Tuff. *Journal of Geophysical Research*, *104*(B9), 20,097–20,122. https://doi.org/10.1029/1999JB900207

Waythomas, C. F., Scott, W. E., Prejean, S. G., Schneider, D. J., Izbekov, P., & Nye, C. J. (2010). The 7–8 August 2008 eruption of Kasatochi Volcano, central Aleutian Islands, Alaska. *Journal of Geophysical Research*, *115*, B00B06. https://doi.org/10.1029/2010JB007437

White, R., & McCausland, W. (2016). Volcano-tectonic earthquakes: A new tool for estimating intrusive volumes and forecasting eruptions. *Journal of Volcanology and Geothermal Research*, *309*, 139–155. https://doi.org/10.1016/j.jvolgeores.2015.10.020

Wicks, C., De La Llera, J. C., Lara, L. E., & Lowenstern, J. (2011). The role of dyking and fault control in the rapid onset of eruption at Chaitén volcano, Chile. *Nature*, *478*(7369), 374–377. https://doi.org/10.1038/nature10541

Wiemer, S., & McNutt, S. R. (1997). Variations in the frequency-magnitude distribution with depth in two volcanic areas: Mount St. Helens, Washington, and Mt. Spurr, Alaska. *Geophysical Research Letters*, *24*(2), 189–192. https://doi.org/10.1029/96GL03779

Woods, A. W., & Koyaguchi, T. (1994). Transitions between explosive and effusive eruptions of silicic magmas. *Nature*, *370*(6491), 641–644. https://doi.org/10.1038/370641a0

Wunderman, R. (2000). Report on Ulawun (Papua New Guinea). *Bulletin of the Global Volcanism Network*, *25*(11)

Wunderman, R.. (2002). Report on Ruang (Indonesia). *Bulletin of the Global Volcanism Network*, *27*(10). https://doi.org/10.5479/si

Xu, W., Jónsson, S., Ruch, J., & Aoki, Y. (2016). The 2015 Wolf volcano (Galápagos) eruption studied using Sentinel-1 and ALOS-2 data. *Geophysical Research Letters*, *43*, 9573–9580. https://doi.org/10.1002/2016GL069820